A Thesis

entitled

Evaluating the Advective Capacity of Regional Groundwater Flow Regimes to Transport Legacy DRP in a Tiled Farm Field of The Maumee River Watershed

by

Matthew McCormick

Submitted to the Graduate Faculty as partial fulfillment of the requirements for the

Master of Science Degree in

Geology

_____

Dr. James Martin-Hayden, Committee Chair

_____

Dr. Daryl Dwyer, Committee Member

_____

Dr. Kevin Czajkowski, Committee Member

_____

Dr. Barry W. Scheuermann, Interim Dean
College of Graduate Studies

The University of Toledo

May 2021

An Abstract of

Evaluating the Advective Capacity of Regional Groundwater Flow Regimes to Transport Legacy DRP in A Tiled Farm Field of The Maumee River Watershed

by

Matthew McCormick

Submitted to the Graduate Faculty as partial fulfillment of the requirements for the Master of Science Degree in
Geology

The University of Toledo

May 2021

Recent research investigating the contributions of non-point legacy dissolved reactive phosphorus (DRP) sources to DRP loading in the Maumee River watershed has relied heavily on edge of field methods. While edge of field methods consider the hydraulic and chemical parameters of tile drainage and overland flow, these studies neglect to consider the field-scale groundwater flow regimes which control the mobilization and advection of DRP to tile drains. Understanding the field-scale advective capacity of groundwater can aid in the assessment and modeling of the impacts of legacy sources on watershed DRP loading. A tile drained farm field with legacy soil P accumulation resulting from decades of biosolid applications within the Maumee River watershed was selected as a study site to evaluate the advective capacity of two groundwater flow regimes: rapid return flow (RRF) and slower groundwater baseflow (SBF). 15 piezometers were installed throughout the farm field to characterize the unconfined aquifer, monitor the potentiometric surface, and permit groundwater sampling. Hydrograph separation of piezometer and tile drain hydrographs yielded the

RRF and SBF components of groundwater and tile discharge. The legacy P source in the soil profile was characterized by sampling the soil profile at increasing depths.

Results show significant legacy soil P accumulation in the near surface soil profile (100-300ppm soil test phosphorus, 0-60cm), with a stratification of concentrations that decreased as depth in the soil profile increased. Elevated groundwater DRP concentrations observed after recharge indicate that gravity drainage is mobilizing legacy P sequestered in the soil profile. The RRF component of piezometer hydrographs was found to transport considerably less DRP than SBF, accounting for 13% of total discharge and 11% of DRP mass transported. This regime dynamic was also present in groundwater and tile drain discharge as baseflow. The total DRP mass discharged by the tile drain (357.65g) was found to be less than the mass transported by groundwater to the tile drain (388.80g), raising the possibility of sequestration as DRP mass moves through the unconfined aquifer.

The results of this study highlight the advective capacity of groundwater flow, especially SBF, to transport legacy DRP to tile drains. RRF was found to be a minor contributor to DRP mass input and advection due to limited discharge capacity. SBF is the dominate flow regime in legacy DRP systems due to slow recession of head and prolonged interaction with the soil P source. In traditional systems, RRF is the flow regime often linked to DRP mass transport. However, these results show that SBF dominates DRP mass transport in legacy systems due to the nature of the P source and the process of mobilization. Given these results, it is recommended that future research consider regional groundwater flow regimes when assessing the impact of non-point legacy DRP sources. To date, no studies have evaluated the capacity of groundwater and

its associated regimes for advective potential in legacy systems. Understanding the field scale hydraulic mechanisms controlling legacy DRP runoff can aid in the development of mitigation measures and conservation techniques to decrease DRP loading in the Maumee River watershed.

Acknowledgements

I would like to thank Amar Kolapkar for his hard work and dedication to this project and for his friendship during my graduate tenure. This research would not have been possible without his contributions. A special acknowledgement is reserved for Steven Murphy who helped in the design of the standpipe weir and with many more instruments and equipment needed for this study. A sincere thank you to my wife Kayla, and my friends and family who never stopped supporting me and cheering me on.

A very special thank you to my advisor, Jamie. You believed in me when others did not. Thank you for sharing your knowledge, guidance, and friendship. I can confidently say I've had the best advisor a graduate student could ask for.

Table of Contents

List of Figures

Fig.

Chapter One

Introduction

Perched on the edge of the midwestern corn belt, the Lake Erie Basin (LEB) has endured persistent water quality issues stemming from intense agricultural land use. Despite wide scale adoption of land and crop best management practices (BMPs) such as no-till crop management, winter cover crops, crop rotations, and 4R nutrient stewardship, non-point agricultural sources remain the largest contributor to phosphorus (P) loading in the watersheds of the LEB (Arhonditsis *et al.*, 2019; IJC, 2018). Evidence is mounting that past mitigation strategies which successfully reduced total phosphorus (TP) loads are now exacerbating dissolved reactive phosphorus (DRP) loading to Lake Erie delivered by the Maumee River (Guo *et al.*, 2021; Kast *et al.*, 2021; Smith *et al.*, 2015c). More bioavailable than TP, increased DRP loading has been identified as a major catalyst behind the re-eutrophication of Lake Erie (Baker *et al.*, 2014; Baker *et al.*, 2019; Kane *et al.*, 2014; Michalak *et al.*, 2013). DRP is the dissolved portion of TP and is defined as the P remaining in a sample after filtration through a 0.45-µm pore diameter filter.

Jarvie *et al.* (2017) discovered that large scale adoption of the high-residue crop BMP 'no-till' is likely contributing to increasing DRP loads delivered by the Maumee River watershed (MRW). The no-till BMP directs farmers to leave crop residue in place after harvesting as opposed to tilling and inverting the soil to incorporate crop residue. No-till crop management promotes the development of soil structure by preserving the soil profile while crop residue improves soil health, thus preventing erosion and limiting surface runoff (Islam and Reeder, 2014). However, preservation of the soil profile inadvertently fosters the development of vertically stratified soil P (Baker *et al.*, 2017; Jarvie *et al.*, 2017). Vertical stratification of soil P results from the breakdown of crop

residue coupled with surficial P applications that were not incorporated into the soil. Over time, P leeched from crop residue and unincorporated fertilizers accumulate at the soil surface in elevated concentrations (Baker *et al.*, 2017; Osterholz *et al.*, 2020b). Infiltrating direct and indirect precipitation mobilize P accumulations at the soil particle surface, resulting in a vertically stratified distribution of soil test phosphorus (STP) concentrations in the soil profile (Hanrahan *et al.*, 2021).

Stratified elevated STP concentrations are commonly found near the soil surface (0 to 5cm) however, stratification of significant STP concentrations can extend further down the soil profile (5-60cm) and into the saturated zone (Domagalski, 2012). Soil P that has accumulated in this manner has been termed "legacy P" in a reference to the legacy of the land or crop management practice which fostered the P accumulation. Legacy P is an historically overlooked source of DRP that is mobilized by soil-water and transported off farm fields via the extensive network of subsurface tile drains in the watersheds of the LEB (King *et al.*, 2015; Muenich *et al.*, 2016; Sharpley *et al.*, 2013). Due to the poorly drained glacially derived soils present in the MRW, extensive subsurface tile drainage is required to facilitate adequate drainage. Subsurface tile drainage drastically expedites field drainage creating 'flashy' flow events that have modified the natural hydrology and hydrogeochemistry of Lake Erie's watersheds (King *et al.*, 2018; Williams *et al.*, 2016a). Coupled with increasingly intense spring storms and rapid field drainage, legacy P sources have the potential to increase DRP loading at the basin scale.

Current research shows the development of legacy P in cash crop fields of the LEB is a potential consequence of not only the no-till BMP but a combination of other

BMPs as well (Gatiboni *et al.*, 2020; Jarvie *et al.*, 2017; Liu *et al.*, 2019b). It is also not uncommon for the farmers who choose to adopt BMPs to implement many or all BMPs mentioned in this paper simultaneously which further increases the likelihood of legacy P accumulation (Burnett, 2015). Winter cover crops, an increasingly adopted BMP in the LEB and MRW, has also been found to exacerbate P soil stratification (Ni *et al.*, 2020). Winter cover crops planted in the MRW include winter wheat, buckwheat, and clover which are used as mulch or, more commonly, left on the field as crop residue (Burnett *et al.*, 2018). Crop residue from winter cover crops adds to the near surface buildup of organic residue and is commonly used in conjunction with no-till and crop rotation. Additionally, research has suggested that due to the freeze-thaw cycle in colder climates, winter cover crops produce more P when decaying, increasing the potential for P leeching accumulation at or near the soil surface (Cober *et al.*, 2018; Liu *et al.*, 2019a).

Crop rotation is another BMP aimed at reducing surface erosion, improving soil health, and fixing excess soil nutrients to reduce surface TP runoff. However, research suggests this BMP increases DRP losses by also compounding the accumulation and stratification of soil P (King *et al.*, 2016; Yuan *et al.*, 2020). Due to differing crop nutrient needs, P fertilizer applications can often be unnecessary and contribute to P build up at the soil surface when rotating crops, especially in the absence of routine soil testing. The most common crop rotation in the MRW is corn-soybean, of which corn crops require more P than soybean crops and produce more P-rich crop residue (King *et al.*, 2016). Rotating these crops can often create a nutrient cycle where more P is sequestered in the soil than taken up by crops, especially when crop rotation is used in conjunction with other BMPs (Smith *et al.*, 2015a).

While BMPs are a component of the catalysts exacerbating DRP runoff in the MRW, it is important to note that many other factors are also causing a release of DRP from legacy fields. A lack of acidic rain following the implementation of amendments to the Clean Air Act is changing soil pH, creating the perfect geochemical environment for DRP release from sequestered legacy soil sources (Smith *et al.*, 2017). A changing climate in the LEB and MRW has caused increases in annual precipitation totals and the intensity and frequency of spring storms, altering the hydrologic dynamics in these watersheds. A prolonged history of biosolid applications on many fields have created legacy P sources. Increased DRP runoff is catalyzed by a confluence of factors, of which BMP adoption and legacy sources are two of those factors that can be mitigated by human intervention at the field scale.

Considering the prevalence of subsurface tile drainage in the MRW, the large-scale adoption of BMPs, and a climate forecasted to become more humid, non-point legacy P sources have the potential to increase DRP loads delivered to Lake Erie (King *et al.*, 2015). Current and year to date studies investigating the impact of legacy P on DRP concentrations present in agricultural subsurface runoff focus only on the catchment or watershed scale using edge of field data collection methods (Daniels *et al.*, 2018; King *et al.*, 2016; Osterholz *et al.*, 2020a; Pease *et al.*, 2018; Sharpley *et al.*, 2009; Smith *et al.*, 2015b). Tile drain effluent chemistry and discharge rate, tillage type, and soil characteristics are considered in these studies, yet edge of field data only encompasses the water quality and hydraulic parameters of tile drainage, ignoring the advective capacity and role of groundwater flow in transporting legacy DRP.

To fully evaluate the potential for legacy P to increase DRP loads in tile drain effluent, the fate and transport of legacy P from its source in the soil profile to discharge by tile drains needs to be assessed at the field scale. Given the hydraulic dynamics of the system, infiltration of precipitation and gravity drainage to the water table (groundwater recharge) and groundwater flow must be the dominant factors controlling the mobilization and transport of DRP from legacy sources. Quantifying the dynamics of groundwater recharge, field-scale groundwater flow paths, and groundwater discharge to tile drains is key to understanding the underlying mechanisms behind the mobilization and transport of legacy P.

Therefore, the goals of this study are to investigate soil P mobilization and DRP transport in a legacy field managed with BMPs by evaluating the spatial and temporal parameters of two groundwater flow and transport pathways to subsurface drainage: rapid return flow (RRF) and slower groundwater baseflow (SBF). The individual objectives to complete these goals are: (i) characterize the legacy source of DRP in the soil profile (ii) identify infiltration and gravity drainage as the mechanism of DRP transport to the water table (iii) estimate the DRP mass transported to groundwater (iv) use piezometer hydrographs to separate RRF from SBF (v) calculate groundwater discharge (vi) calculate the timing and volume of DRP mass discharged by the tile drain (vii) assess the mass balance between groundwater and tile effluent DRP mass.

It is postulated that SBF and its associated regimes are the primary advective mechanism transporting legacy DRP to tile drains at the field scale. RRF represents rapid groundwater recharge and return of shallow groundwater flow to the tile drain. This rapid event flow is short in duration which limits the volume of discharge and therefore

advective capacity. While event flow is known to exhibit higher TP and DRP concentrations, it is theorized that in legacy systems slower flow regimes would transport more DRP mass over time. . Groundwater recharge that passes slowly through the soil matrix facilitates soil-water geochemical interactions which catalyze the desorption of P from soil particles. Depending on the extent of STP stratification, slower groundwater flow (SBF) could act as the dominate mechanism through longer residency time within stratified material. Additionally, during the wet season when the water table rises to its maximum elevation, legacy P potentially stratified within the capillary and unsaturated zone could mobilize through geochemical interactions with groundwater that usually does not saturate those zones.

Chapter Two

Methodology

Site Description & Geologic Setting

The study site is a row crop farm field operated by the Lucas Soil and Water Conservation District (LSWCD), located 1.5 miles due south of the village of Whitehouse in southwestern Lucas County within the Blue Creek Conservation Area (Fig. 1). Located within the lower MRW, the field was selected for its unique and extensive conservation management history and high STP concentrations despite a prolonged period of no P applications. Since 1992, the field has served as a LSWCD managed farm field used to demonstrate the effectiveness of BMPs while maintaining crop yields. BMPs historically implemented at the site include no-till, conservation till, crop rotation, 4R nutrient stewardship, and winter cover crops. No P fertilizers have been applied to the field since 1992 considering high STP concentrations resulting from nearly a century of biosolid applications (LSWCD, verbal communication 2019). Tri-State Fertilizer Recommendations for corn, soybeans, wheat and alfalfa fields suggest ceasing P input at STP concentrations above 40 ppm (Culman *et al.*, 2020). STP concentrations of 102 ppm were observed on site in 2019 during a biannual agronomy soil test. A soy/corn crop rotation has been followed for the past seven years with previous crop years consisting of corn according to LSWCD staff.

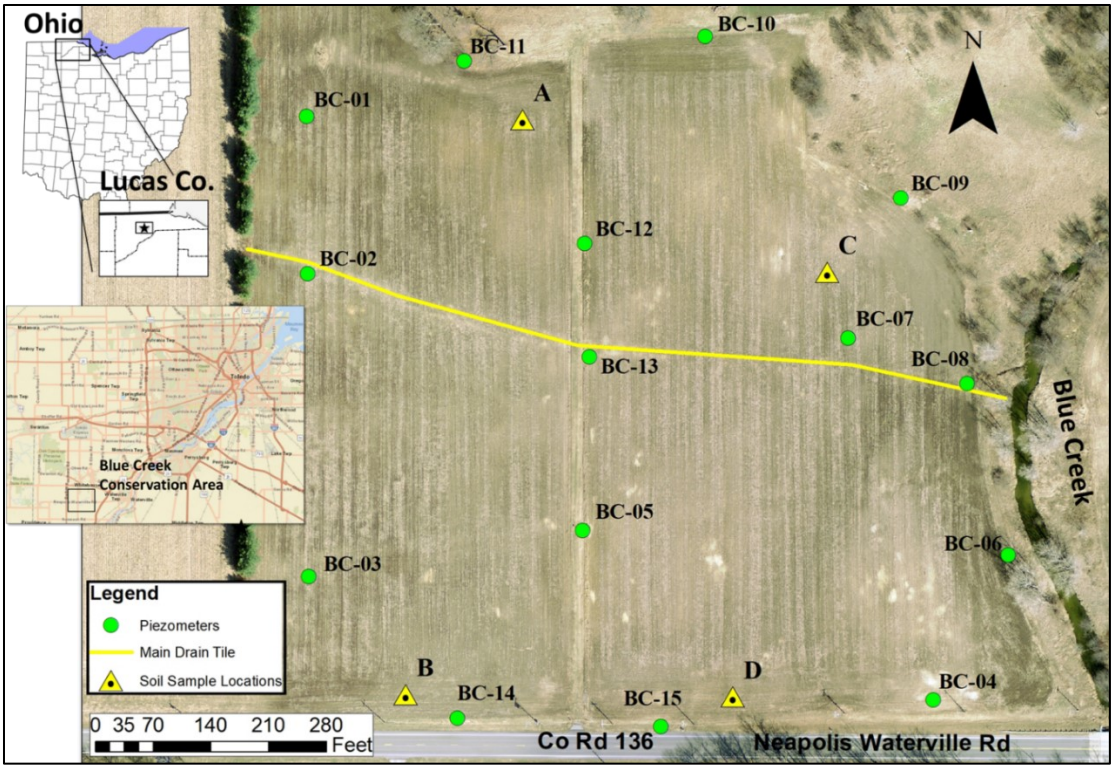

Fig. 1 The study area at the Blue Creek Conservation area 1.5 miles south of the village of Whitehouse. Green dots represent piezometers and yellow triangle soil sample locations. The main tile drain is outlined in yellow and runs from west to east across the field.

The bedrock of the study area consists of Lucas Dolomite overlain by clayey Wisconsin till capped with glaciolacustrine sandy silt to silty sand. Lenses of sandy to silty clay heterogenize the sandy silt to silt sand unit. On the west side of the field, a thin (<2 ft) layer of fine to medium sand overlays the sandy silt/silty sand (Fig. 2). The bedrock elevation is high in this area of northwest Ohio, with thin surficial glaciolacustrine and glacial deposits (<50 ft). Bedrock is exposed at the surface 1,500 ft to the north east of the study site and 1.07 miles to the north within the city limits of Whitehouse. A series of now abandoned quarries exploited the bedrock exposure in this area for aggregate and stone quarrying. The maximum thickness of the glaciolacustrine and till deposits are 39 ft at the western extent of the field and thin to the east as bedrock

elevation increases. The sandy silt to silty sand unit is consistent in an average thickness of 6ft within the bounds of the study site.

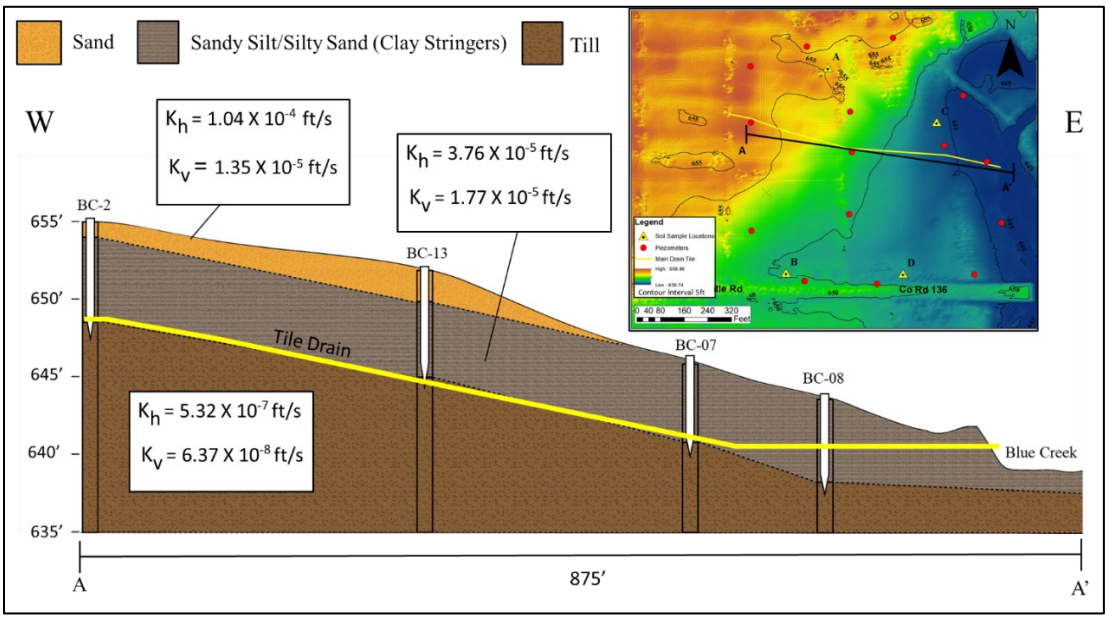

Fig. 2 West to east cross section of study area lithology constructed from bore logs. Hydraulic conductivities (vertical and horizontal) for each unit are given in breakaway boxes. Bedrock is at an average elevation of 620 ft in the area. Inset is a digital elevation model (DEM) of the site topology, where warm colors denote higher elevations and cool colors lower elevations. The transect A to A' denotes the physical extent and orientation of the cross section.

The soil profile of the site consists of level to gently sloping silty clay loam overlain by loamy medium to fine sand capped by humus. The west of the field has a profile dominated by fine to medium friable loamy sand in the first few cm of the pedon, formed from glaciolacustrine shoreline parent deposits. The National Cooperative Soil Survey (NCSS) soil units present in the field are the Ottokee fine sand, Bixler loamy fine sand and Sloan loam with slopes ranging from 0 to 6%. These soils are similar to other glacially derived soils present in the lower MRW apart from the appearance of fine sand which is restricted to a limited distribution in Lucas, Fulton, and Henry counties.

Hydraulically, the clayey Wisconsin till serves as the underlying aquitard and the silty sand/sandy silt constitute the unconfined aquifer in this system. Blue Creek bordering the east of the field and a storm ditch running along the road to the south serve as hydraulic boundaries. The tile drain network was delineated using multi-spectral ariel image analysis by examining drainage patterns present in ariel images captured after precipitation, a common practice for tile drain delineation (Andrade, 2013; IGS, 2015; Thompson, 2010). Delineation accomplished with aerial imagery was compared to LSWCD historical records and AT&T Communication Line schematics (a fiber optic communications line runs through the field from west to south east) for verification. It was determined that a single tile drain is present in the center of the field running west to east which corresponds to LSWCD records and current staff knowledge. This tile drain serves as a hydraulic boundary dividing the field into two sections: the north and south hydraulic zones. The tile drain was installed at an average depth of 6 ft above the impermeable till. Depth of the tile drain was verified in the field using a tile probe.

During the spring of 2020 (March through May), this site was investigated for DRP transport from potential legacy sources. Precipitation data for the period was obtained from the NOAA weather station located at the Toledo Airport (KTOL), 6.4 miles north of the site. Precipitation totaled 9.8 inches during the period of 3/1/2020 to 5/31/2020. The spring and summer months represent the nutrient loading season in the MRW (March 1st-July 31st), when spring planting and fertilizer applications coincide with frequent and intense precipitation.

Groundwater & Tile Effluent Monitoring

Fifteen 1 ¼ inch diameter piezometers were installed in a tessellated network throughout the field to monitor the potentiometric surface (water table), permit groundwater sampling, and allow for the characterization of the unconfined aquifer (Fig. 3). The piezometers consist of a PVC casing coupled to a finely slotted (.006 in wide) 3 ft long screened section that creates a hydraulic connection with the unconfined aquifer to measure heads and collect groundwater samples (See Appendix A). Piezometers were installed by hand auguring a 3½ inch diameter borehole into the saturated zone and placing the coupled PVC casing and screened section into the borehole. The slotted section was then surrounded with fine silica sand to ensure a uniform hydraulic connection and prevent the screen from clogging. A 1½ to 2 ft diameter plastic sheet collar was secured to the PVC casing at least one foot below the land surface to limit leakage down the side of the casing. Piezometers were installed in a tessellated pattern to maximize the area of the site covered by sets of three wells, allowing for application of a 3pt problem (Vacher, 1989) to determine the direction and magnitude of the hydraulic gradient and horizontal groundwater flow paths.

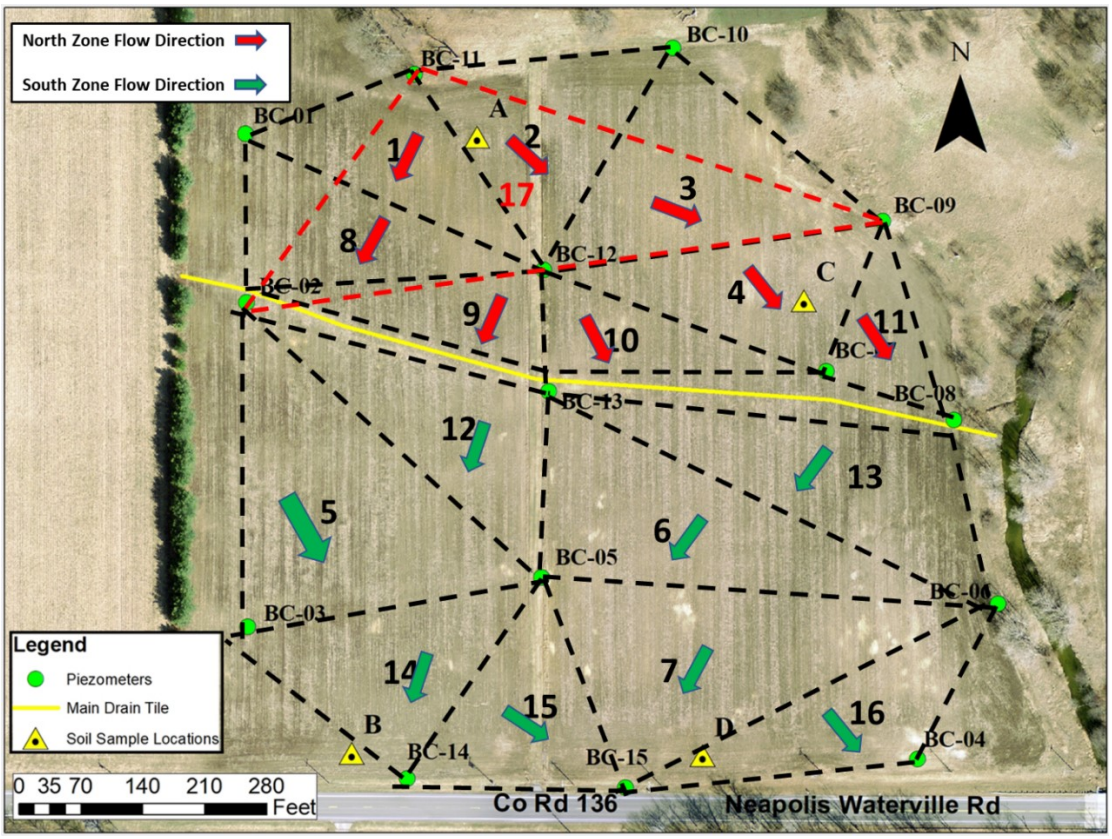

Fig. 3 Tessellated 'triangles' of three piezometers encompassing the study site. Within each triangle's spatial geometry, the flow direction and hydraulic gradient for the saturated thickness of the unconfined aquifer is calculated. Triangle 17 is denoted by a red dotted line and covers a large area with a 15-minute hydraulic head resolution. The tile drain forms a hydraulic boundary separating the field into two hydraulic zones to the north and south of the tile drain.

On a weekly and bi-weekly basis in the spring of 2020, hydraulic heads were measured using a Solinst 101 water-level meter for all piezometers. To prevent cross contamination, the water level meter sensor was rinsed with reverse-osmosis filtered water after each measurement. Three Sonlinst Leveloggers and 1 Van Essen CTD-Diver datalogging pressure transducers were installed in BC-02, BC-09, BC-11 and BC-07 in the north hydraulic zone to collect head elevation and temperature data at 15-minute intervals. Submerged pressure transducer data were compensated using onsite 15-minute

barometric data collected with a Solinst Barologger and Van Essen Baro-Diver placed in BC-02 and BC-11, respectively.

The rate and volume of tile drainage was monitored using a modified compound V-notch weir design and standpipe apparatus consisting of an 8 in PVC elbow which was placed on the tile drain outlet and a 3 ft section of 8 in PVC that serves as the standpipe. The standpipe section was cut into a 22.5° V-notch tapering down to a narrow rectangular slit 8 in long and 0.3 inches wide to accommodate both high and low flows over the weir. By measuring the fluctuating head in the standpipe (head behind the weir), volumetric discharge over the weir is calculated (Interior Dept., 2001). A CTD-Diver datalogging pressure transducer was placed in the standpipe to continuously monitor the head in the standpipe. A rating curve to calibrate weir discharge calculations was developed by manually measuring discharge over the weir using a large graduated cylinder under both high and low flow conditions.

Sampling & DRP Analysis

Sampling of groundwater was conducted weekly throughout the study period with high frequency sampling during storm events. Grab samples of groundwater were collected from piezometers using a clean PVC bailer and placed into a clean 50 ml BPA free plastic centrifuge tube. The PVC bailer was rinsed with R.O. water before and after each sample was collected to prevent cross contamination between piezometers. Samples were then placed in an iced cooler at or near 4°C before being refrigerated in the lab at 4° C pending analysis within 24 hours.

Tile drain effluent was automatically sampled with a Hach model 900 refrigerated automatic sampling unit on a regular 8-hour basis and on a 2-hour basis during two spring storm events. The Hach auto-sampler sampled tile effluent in situ via a 17 ft, 1½ in diameter section of PVC tubing that was fitted to the standpipe weir using a brass fitting. A programmed rinse cycle was performed by the sampler before sample extraction to provide a representative sample and remove any contaminates. Samples collected by the Hach sampler were stored in clean 1-liter BPA free plastic containers within the refrigerated compartment of the sampler before being transferred to clean 50ml centrifuge tubes and placed in an iced cooler pending transport to the lab. Samples of Blue Creek were collected periodically upstream and downstream of the tile drain outlet using a PVC bailer or by hand before also being placed in a clean 50 ml centrifuge tube.

Tile effluent, Blue Creek, and groundwater samples were analyzed per procedures consistent with EPA method 365.3 (EPA, 2008) within 24hrs of collection using Hach PhosVer 3 ascorbic acid reagent pillows and a Hach DR2000 spectrophotometer at the University of Toledo Hydrogeology Laboratory. Samples were first removed from refrigeration and allowed to reach room temperature before being centrifuged at 3,000 rpm for 15 minutes to remove particulates. Samples were then filtered through a 0.45-µm pore-diameter membrane filter using a vacuum assisted gravity drainage apparatus to remove any remaining particulate P. By definition, DRP is the P that remains after all particulate P is filtered from a sample using a 0.45-µm membrane filter (Pierzynski, 2000). A PhosVer 3 ascorbic acid reagent pillow packet was then added to 25ml of centrifuged and filtered sample and magnetically stirred for 2 minutes before being analyzed by the Hach DR2000 spectrophotometer for DRP concentration (mg/L).

After analysis, observed DRP concentrations for groundwater and tile effluent samples were linearly interpolated in order to correspond to 15-minute measurements of head in piezometers and 15-minute tile drain discharge data.

Characterizing Legacy P as the Source of DRP Transported to GW

To characterize the source of legacy P inputs to the groundwater, the soil profile and near surface lithology were sampled at increasing depths of 5 cm, 10 cm, 30 cm, 61 cm, 91cm and upon encountering saturated conditions at four representative locations within the field near BC-11, BC-09, BC-14 and BC-15 (Fig. 1). Typically, the upper 5 to 10 cm of the soil profile will exhibit the highest concentrations of STP stratification (Baker *et al.*, 2017). However, considering the long history of biosolid fertilization and BMP implementation at this site, it was hypothesized that STP stratification extends to lower depths. Samples were collected following NCSS field collection guidelines using a hand auger before being bagged and promptly shipped to SureTech Labs of Columbus, Ohio for Mehlich-3 STP analysis. The relationship between depth in the soil/lithology profile and STP concentration was then assessed to determine the vertical extent of STP stratification.

DRP Transported to and Recharging Groundwater

By correlating DRP concentrations in the groundwater to groundwater recharge episodes, the mechanisms mobilizing and transporting P to the groundwater were identified. A general increase of DRP in the shallow groundwater during and

immediately after groundwater recharge would indicate mobilization and transport by gravity drainage to the groundwater.

To estimate the DRP mass transported by groundwater recharge and subsequent discharge, average specific yield (S_y) is first estimated using the Water Table Fluctuation (WTF) method (Crosbie *et al.*, 2005) for the storm peaks in piezometer hydrographs. Using hydrograph analysis as outlined by the WTF method coupled with recharge (R) data, S_y is calculated with (eq. 1), where R is recharge in feet and Δh is the change in head in feet from the last recession to the peak of the storm event in question. When the soil is at field capacity (preceding a recharge event), R was approximated as precipitation given the thin unconfined aquifer and shallow potentiometric surface. However, it should be noted that if some precipitation is retained by soil moisture deficit or discharged by overland flow, precipitation would be an overestimate of R.

$$[1] \quad S_y = R / \Delta h$$

Average S_y was calculated for three piezometer hydrographs, BC-02, BC-09, and BC-11 using multiple storm peaks within each hydrograph. Once average S_y is known, the volume stored in specific yield per unit area (V', ft^3/ft^2) can be calculated by multiplying the head as measured from the bottom of the aquifer (h) by S_y for each 15-minute measure of head, $V'=h*S_y$. In eq. 2, increasing head (Δh) indicates groundwater recharge calculated as V' (ft^3/ft^2). Fifteen-minute V' estimations are then multiplied by linearly interpolated groundwater DRP concentrations, C_R (g/ft^3), to give the mass input per unit area (M_R in g/ft^2) of DRP transported by R.

$$[2] \quad V' = \Delta h * S_y$$

Mass Transport by Rapid Return Flow & Groundwater Baseflow

A modification of the Meyboom method (Meybloom, 1961) for estimating groundwater recharge from a storm hydrograph ($\Delta V'$ vs. time) was used to separate the rapid return flow by groundwater (RRF) and slower groundwater baseflow (SBF) components of the V' hydrograph. Derivations of the baseflow equation and the rising-limb equation where used to separate the SBF (V'_b) and RRF (V'_r) flow paths. The baseflow recession constant (a) and the rising-limb constant (a') were calculated using eq. 3 and eq. 4 respectively, where V_1 and V_2 are two points along the recession line at time t_1 and t_2. V'_m is the minimum low flow before the beginning of the storm at time t_m.

[3] $$a = \ln (V_1 / V_2) / (t_2 - t_1)$$

[4] $$a' = \ln (V'_m / V'_o) / t_m$$

SBF at the peak of the hydrograph (V'_o) was calculated using eq. 5 and was then subsequently used to extrapolate V'_b backward towards the storm peak in question. V'_b was calculated using eq. 6. V'_r was calculated by subtracting V'_b from the total V' of the hydrograph.

[5] $$V_o' = V_1 \cdot \exp (a \cdot t_1)$$

[6] $$V'_b = V'_o \cdot \exp (-a \cdot t)$$

With the two flow components separated, mass output of SBF and RRF (M g/ft^2) is calculated by multiplying V'_b and V'_r by interpolated groundwater DRP concentrations (C_R g/ft^3).

Calculation of Groundwater Discharge and DRP Mass Transport

The hydraulic conductivity (K) of the unconfined aquifer was measured with a series of Lefranc pocket (Marsily, 1985) pump tests (Eq. 7 & 8), where D is the diameter of the bore hole, *l* is the length of the pocket (i.e. the length of the saturated piezometer screen) and Q is the discharge in ft^3/sec. Having an estimate of K, a form of the Dupuit equation is then applied to calculate hydraulic flux (q_g) and volumetric discharge (Q_g) within triangles of piezometers. The Dupuit equation is a form of Darcy's Law (Fetter, 2000) modified for horizontal flow within an unconfined aquifer (Eq. 9). Where b_{av} is the average saturated thickness of the unconfined aquifer in the triangle and *w* is the length of tile drain adjacent to the triangle that groundwater is discharging from. Average saturated thickness of the unconfined aquifer was calculated by subtracting the measured head at each piezometer from the elevation of the aquitard and averaging the results.

[7] $$z = \ln\left(\frac{2l/D}{2\pi l/D}\right)$$

[8] $$K = (z / D) * (Q / \Delta h)$$

[9] $$q' = Q / w = K * b_{av} * \text{grad.h}$$

An elementary three-point problem vector analysis (Pizarro, 1988) was utilized in Microsoft Excel 2016 to determine the gradient of the potentiometric surface (grad.h) and azimuth direction of flow within each triangle of piezometers. The flux q_g, was calculated for each triangle by multiplying K by the average aquifer thickness within a given triangle of piezometers and the calculated grad.h. Volumetric groundwater discharge (Q_g) to the tile drains was then calculated by multiplying q_g by the length of tile drain adjacent to the triangle.

The DRP mass (M_g g/d) transported by groundwater flow to the tile drain was calculated by averaging the measured DRP concentration within the piezometers of each triangle and multiplying that average by the Q_g. The rate of M_g advection was calculated for every triangle of piezometers during 4 to 8 periods depending on the availability of well data (the unconfined aquifer is seasonally ephemeral which rendered some piezometers dry, thus creating gaps in head data).

The Meyboom hydrograph separation methodology applied to individual piezometer hydrographs was also applied to the calculated triangle Q_g hydrograph for a large triangle of piezometers, triangle 17 (BC-02, BC-11, BC-09), in order to separate the RRF and SBF flow path components of groundwater discharge. The lateral movement of DRP mass was assessed by calculating the magnitude of M_g transported from one triangle of wells to an adjacent triangle along horizontal flow paths.

Quantifying DRP Mass Discharged by Tile Drainage

The augmented Meyboom method of hydrograph separation described above was also applied to the hydrograph generated by tile drain discharge (Q_T L/hr) to separate RRF and baseflow (slower, intermediate flow) flow paths. Observed tile effluent DRP concentrations were linearly interpolated to coincide with 15-minute Q_T measurements. During two storm events (4/9/20 and 5/19/20), tile effluent was automatically sampled on a high frequency 2-hour basis to better assess storm mobilization and transport of DRP via subsurface drainage. The DRP mass rate discharged by tile drainage (M_T g/hr) was calculated by multiplying interpolated DRP concentrations by Q_T for each measurement of Q_T.

Chapter Three

Results

Groundwater and Tile Effluent DRP

DRP concentrations measured in both groundwater and tile effluent often exceeded the EPA phosphorus criteria (0.076 mg/L) for TP in the ecoregion which encompasses the LEB (EPA, 2000). There are no state or federal criteria for DRP concentration in surface or groundwaters, so the EPA criteria for TP in streams and rivers is used as a proxy. Considering that TP includes both particulate P and DRP, measures of DRP concentrations that met or exceeded the EPA TP criteria were considered elevated. During the study period, average groundwater DRP concentrations were found to exceed 0.25 mg/L while tile drain effluent DRP concentrations averaged 0.06 mg/L with higher concentrations observed during storm events (>0.20 mg/L, see Appendix B). An average DRP concentration of 0.07 mg/L was measured in Blue Creek, with increases in DRP concentration positively correlated with recharge frequency and intensity (see Appendix B).

Source, Mobilization, and Transport of Legacy DRP in Groundwater

STP concentrations present in the soil analyses exhibited a vertical stratification of concentrations, with STP concentrations decreasing as depth increased in the soil/lithologic profile at each sampling site (Fig.4). STP concentrations greater than the Tri-State Recommended “no application limit” for P (>50 ppm) were observed at a depth

of 60 cm at soil sampling site B while sites A, C, and D exhibited reduced concentrations at depths greater than 60 cm. Below 60 cm in the soil/lithologic profile, STP concentrations were less than 50 ppm with an average of 28.2 ppm, indicating that downwardly mobilized DRP has not extended into the saturated zone. However, site D near BC-15 exhibited a STP concentration of 54 ppm at 90 cm, raising the possibility of P sinks within the field and highlighting the potential for downward migration.

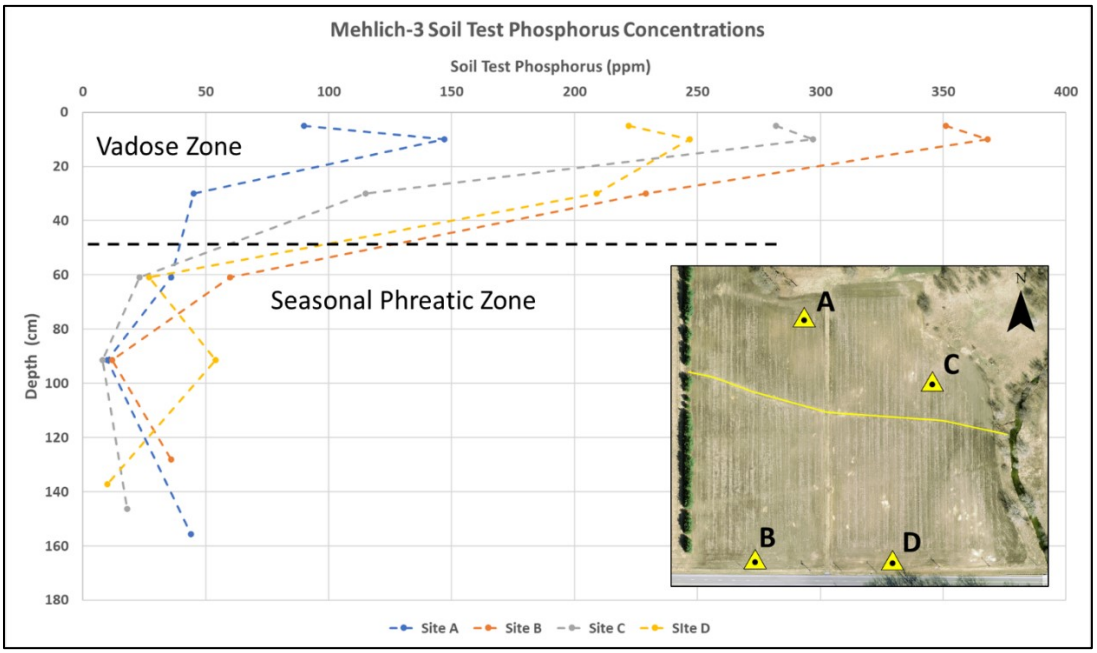

Fig. 4 STP results at increasing depths down the soil profile. Inset map of soil sample locations within the field.

STP concentrations increased closer to the land surface at all sites to an average maximum of 264 ppm in the first 5 cm, well above recommended STP concentrations. Sampling site B exhibited the greatest STP concentrations in the first 5 cm (351 ppm) while samples collected at site A had the lowest STP concentrations at all depths, highlighting the spatial variability in STP concentration. A clear increase in STP concentration from 30 to 5 cm is apparent in all profiles sampled excluding site A, which

exhibited a concentration increase from samples collected at 5 cm and 10 cm. Considering this stratification and magnitude of STP concentrations, the near-surface soil profile from 0 cm to 30 cm is likely the principal source of DRP in this system.

An increase in measured groundwater DRP concentrations was observed after recharge, indicating mobilization of legacy DRP by infiltrating precipitation and gravity drainage (Fig. 5). Piezometers BC-02 and BC-09 exhibited increased groundwater DRP concentrations as head in the piezometer rose, a relationship suggesting the mobilization of legacy DRP by vertical gravity drainage and groundwater recharge. Inversely, groundwater DRP concentrations were observed to decrease with time after recharge (Fig. 5). Given these correlations, mobilization of soil bound DRP and transport to groundwater must be facilitated by gravity driven vertical flow and groundwater recharge.

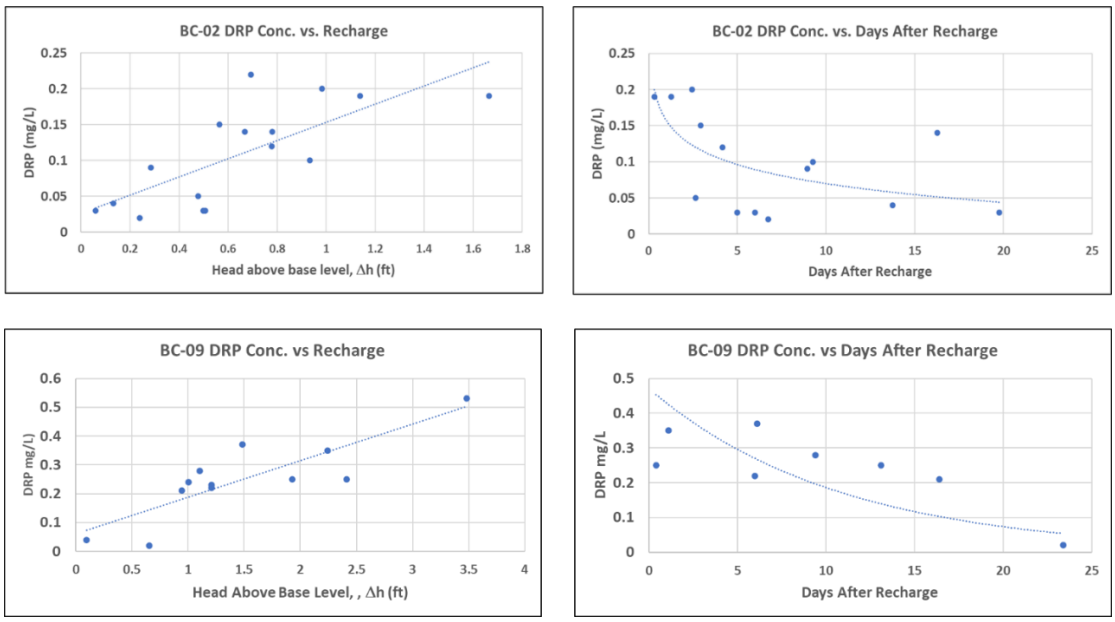

Fig. 5 DRP concentration vs recharge (left) and DRP concentration vs days after recharge (right) for piezometers BC-02 (top) and BC-09 (bottom).

The capacity of the RRF and SBF flow paths to transport DRP was found to be positively correlated to the discharge volumes of the respective flow paths. RRF represents groundwater flow which returns more rapidly to the tile drain by shallow groundwater flow, with peak flows occurring slightly before or at the overall storm peak discharge. Total RRF is contained within the storm peak and declines rapidly as precipitation subsides, resulting in limited discharge from shallow groundwater and limited advective capacity (Fig.6). Calculated DRP mass transported by the RRF flow path is proportional to the discharge volume and accounts for an average 11% of the total DRP mass and 13% of total groundwater discharge during the study period.

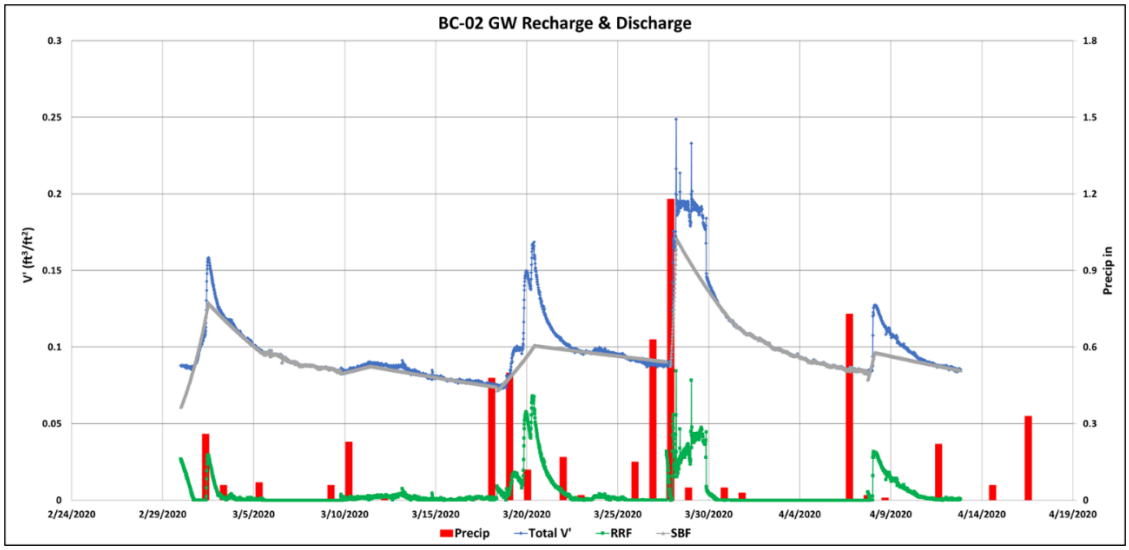

Fig. 6 Hydrograph of piezometer BC-02 separated to give RRF and SBF.

SBF represents a much larger portion of the piezometer hydrograph discharge and therefore accounts for a larger portion of volumetric discharge and mass transport. SBF rises with the rise of the storm peak signifying the input of recharge then slowly decreases in an exponential recession of piezometer head indicating groundwater discharge. Accounting for an average 87% of volume discharge and 89% of total mass transported, SBF is the dominant flow path transporting the bulk of DRP mass in the saturated zone (Table 1). Limited discharge volume and regime duration restrict the capacity of RRF to transport legacy DRP. Inversely, the SBF regime is characterized by a greater discharge volume, resulting in greater advective capacity to transport DRP mass.

BC-02		GW Recharge		Rapid Return Flow		SBF	
	Date	Σ+ΔV' (ft^3/ft^2)	Σ +ΔMass (g/ft^2)	Σ -ΔV' (ft^3/ft^2)	Σ -ΔMass (g/ft^2)	Σ -ΔV' (ft^3/ft^2)	Σ -ΔMass (g/ft^2)
Pk. A	3/2/20	0.068	5.77E-05	-0.027	-2.28E-05	-0.129	-1.10E-04
Pk. B	3/11/20	0.006	6.32E-05	-0.003	-4.06E-06	-0.089	-1.88E-04
Pk. C	3/20/20	0.035	2.38E-04	-0.009	-4.30E-05	-0.093	-5.49E-04
Pk. D	3/28/20	0.115	4.53E-04	-0.032	-1.29E-04	-0.171	-6.81E-04
Pk. E	4/8/20	0.018	9.92E-05	-0.005	-2.60E-05	-0.019	-3.02E-04
Total		0.242	9.11E-04	-0.076	-2.25E-04	-0.501	-1.83E-03
				%V'	%Mass	%V'	%Mass
% of Tot.				13%	11%	87%	89%

Table 1 Change in GW discharge/recharge and DRP mass for piezometer BC-02.

Groundwater Transport of DRP Mass to Tile Drain

By assessing the flow direction within each triangle of piezometers, the overall direction of groundwater flow within the piezometer network was determined to be toward the tile drain in the north hydraulic zone, and away from the tile drain in the south hydraulic zone (Fig. 3). A groundwater recharge zone to the northeast drives the dominant regional groundwater flow from the northeast to southwest. Therefore, the tile drain intercepts groundwater discharge from the north area of the field while the southern area of the field discharges to a roadside ditch and underlying culvert along Waterville-Neapolis Rd. Given this spatial hydraulic dynamic, the northern hydraulic zone was used to assess groundwater transport of DRP mass to the tile drain.

Positive correlation of Q_g and M_g in triangles 9 and 10 directly adjacent to the tile drain demonstrate the relationship between discharge and the DRP mass advected, illustrating that groundwater discharge is transporting DRP mass to the drain (Fig. 7). Triangles covering the spatial extend of the north hydraulic zone exhibit this positive correlation, with M_g increasing as Q_g increases (see Appendix C) . An average calculated

DRP mass of 10.51 g/day is transported to the tile drain from the north hydraulic zone by an average volumetric groundwater discharge of 918.01 ft^3/day.

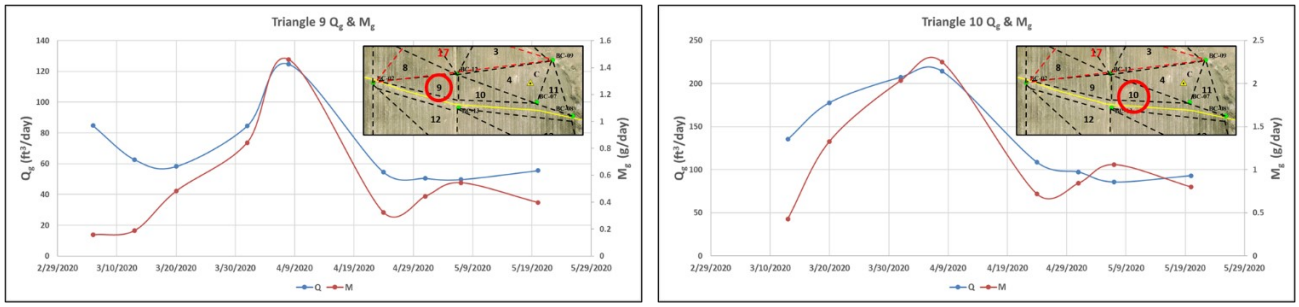

Fig. 7 Hydrographs of triangles 9 and 10 directly adjacent to the tile drain.

The discharge hydrograph of triangle 17 (BC-11, BC-09, BC-02) was used to separate the RRF and SBF flow path components of groundwater discharge in the north hydraulic zone. Results mirrored the flow regime dynamics found with the piezometer hydrograph analyses: where SBF was the dominant flow regime by both volume discharged and DRP mass advected (Fig. 8). The rate of DRP mass transported is found to be directly proportional to the rate of volumetric groundwater discharge. During an 11-day period with two storm events (4/11/20-4/22/20), SBF transported 88% of the total M_g advected (378.29 grams) and total Q_g (10,022.26 ft^3) within the cross-sectional area of the triangle, while RRF conveyed 12% of the total M_g and Q_g, respectively.

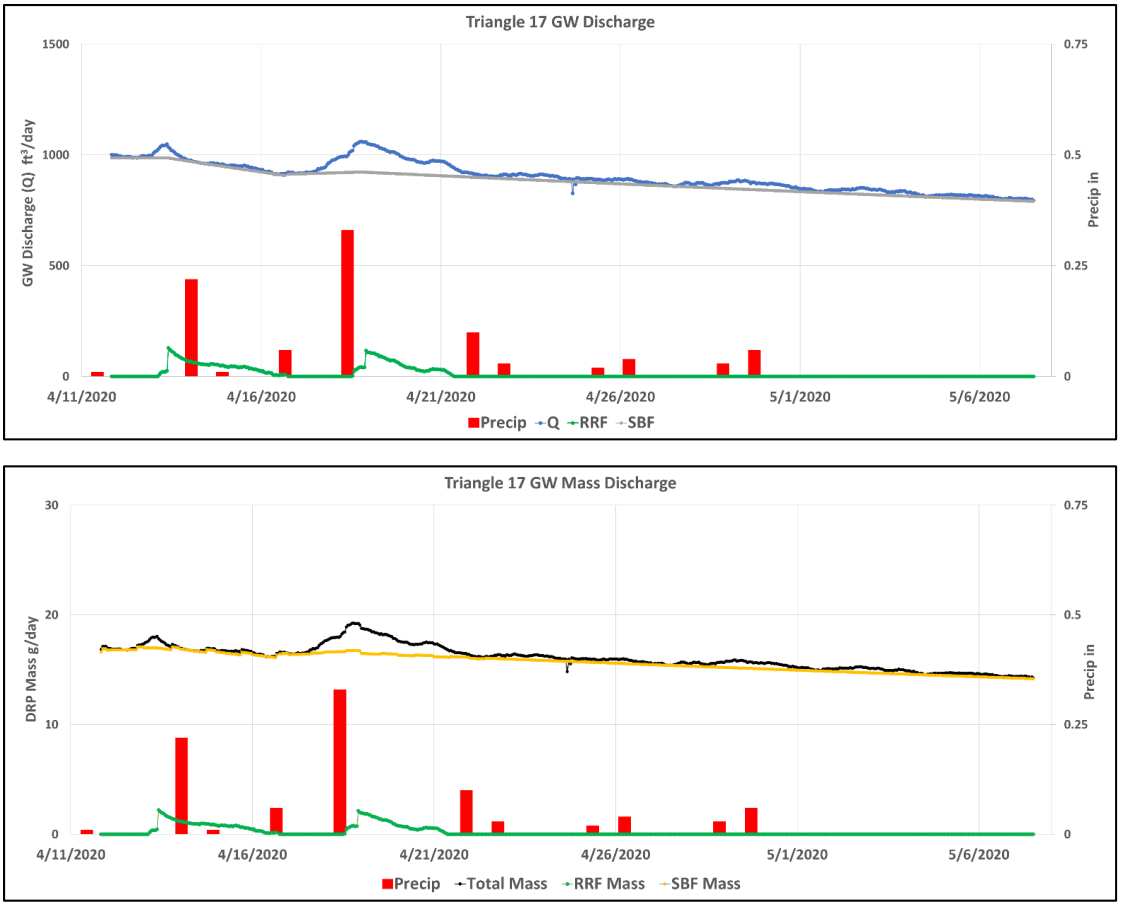

Fig. 8 Above: Triangle 17 hydrograph with RRF and SBF. Below: Triangle 17 DRP mass discharged

Horizontal groundwater advection of DRP in the unconfined aquifer is apparent in the concentration gradient present between triangles 3, 4 and 10 in the direction of groundwater flow shortly after a recharge event on 3/20/20. A M_g rate of 5.97 g/day in triangle 3 decreases to 2.32 g/day in triangle 4 and 1.33 g/day in triangle 10, directly adjacent to the tile drain (see Appendix C). This horizontal concentration gradient parallel to groundwater flow direction demonstrates the continuing advection of DRP to the tile drain by groundwater flow.

Tile Drain Effluent Mass

The rate of tile drain discharge (Q_T) quickly responded to recharge input, demonstrating a rapid increase in Q_T as precipitation intensity increased (Fig.9). A 4/7/2020 to 4/8/2020 storm event caused a response in tile drainage within <25 minutes of precipitation fall. Similarly, a storm on 5/18/2020 to 5/19/2020 resulted in a rapid Q_T response as precipitation amount and intensity increased. These rapid responses are likely dominated by preferential flow in the vadose zone and as well as possible interflow in the vadose zone.

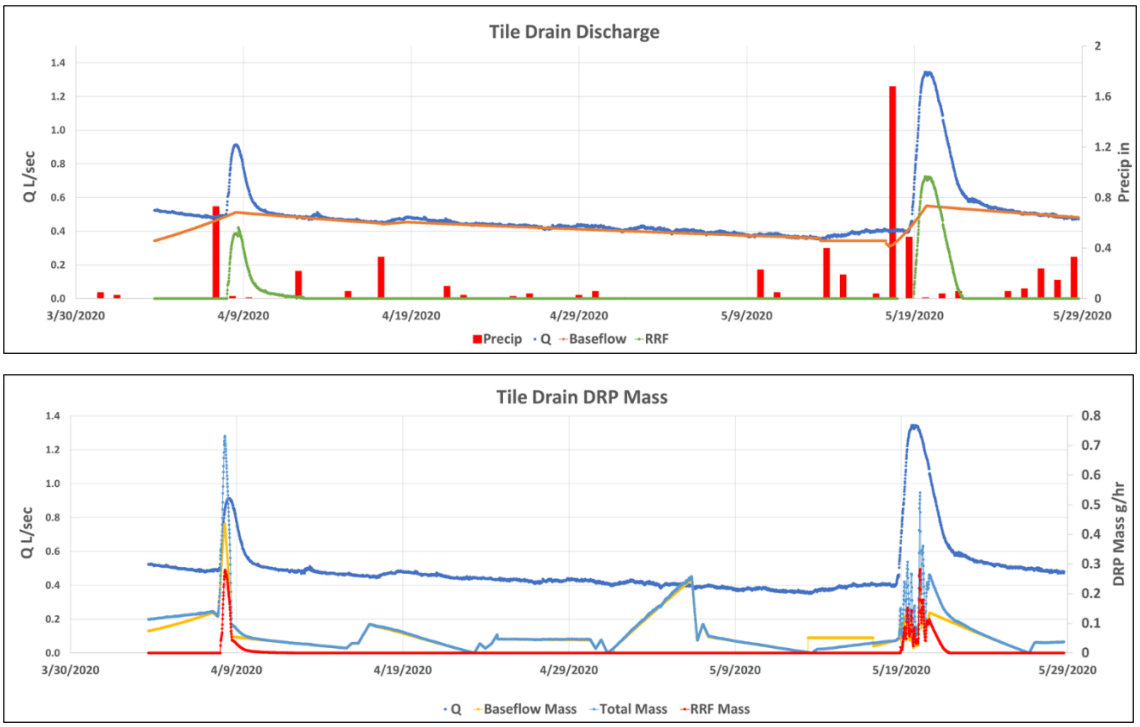

Fig. 9 Tile drain hydrograph (top) with flow components and DRP mass discharged by respective flow components (bottom).

However, similar to previously observed flow path dynamics, the volume discharged and DRP mass transported by RRF is overshadowed by baseflow

contributions. During the period of 4/3/2020 to 5/28/2020, 357.65 grams of DRP was transported by tile drain discharge, of which baseflow accounted for 90% of DRP mass discharged (see Appendix D). In systems where P fertilizers are actively applied, preferential flow is widely accepted to be the primary flow path transporting DRP in subsurface drainage. Conversely, results of this study indicate that baseflow is the primary advective flow regime in legacy systems due to the nature of the legacy DRP source.

Chapter Three

Discussion

DRP Mass Transported by Gravity Driven Infiltration

Mobilized by infiltrating recharge, DRP desorbed from the legacy source in the vadose zone is being transported vertically downward throughout the soil profile at the site, ultimately recharging the phreatic zone. The legacy soil P characterized in the upper 60cm of the soil profile results from decades of biosolid applications (presumably since 1918) until new ownership was assumed in 1992 (verbal conversation with LSWCD, 2019). Yet after ceasing P inputs and adoption of BMPs for a period of 29 years STP concentrations still far exceed tri-state recommendations. Historic STP concentrations were not available for the site beyond 2019. However, LSWCD personnel reported that STP concentrations have been historically high (>100 ppm) at both the study site and in fields throughout the surrounding area of Lucas and Fulton counties, possibly due to a combination of regional BMP adoption and soil characteristics in the region. In a comprehensive study of agricultural vertical P soil stratification in the watersheds of the western LEB, Baker et. al (2017) found that STP concentrations in the first 20cm of the soil profile greater than 56 ppm were present in 75% of watershed soil samples. Concentrations greater than 150ppm were present in 12% of soil samples. STP concentrations ranging from 147ppm to 368 ppm were observed in the first 20cm of the soil profile at this study site, indicating a comparatively substantial accumulation of legacy soil P.

By adopting recommended BMPs that discouraged inverting or disturbing of the soil profile, vertical stratification of STP and development of soil structures that encouraged DRP accumulation and subsequent desorption resulted. Considering the long term adoption of no-till, crop rotation, and cover crops, it can be assumed that while these BMPs have likely limited TP runoff from this site these practices have created an environment positioned to mobilize legacy soil P and increase DRP concentrations in subsurface discharge. While chemical and mineral soil properties control the absorption and desorption of P in soil-water solution, the physical properties of soil structure created by BMPs determine the rate of gravity drainage and duration of soil/soil-water interactions.

The rapid flow component of groundwater recharge highlights the prevalence of preferential pathways in the soil profile of the study area. Preferential pathways result from macropores created by soil organisms and mechanically derived soil structures such as desiccation cracks and alignment of aggregated soil particles (Williams *et al.*, 2016b). These soil water pathways are destroyed when the near surface soil profile is tilled or inverted, yet under conservation BMPs these pathways are preserved. In fields with active P fertilizer applications preferential flow paths are known to contribute to soil-water and groundwater DRP, yet in legacy P systems preferential pathways are evidently less effective at mobilizing DRP from the soil source. Anion exchange with soil particle surfaces in soil-water solution catalyzes the desorption of P from oxide surfaces which increases DRP concentrations in soil water. The RRF component of groundwater recharge and discharge must lack the residency time required to facilitate these

interactions. As a result, rapid event flow is able to desorb very little DRP from soil particle surfaces.

The slower percolation of groundwater recharge through the SBF regime was found to be the dominate pathway transporting DRP mass to groundwater due to interactions with soil particles in the soil matrix. Depending on the pH and dissolved oxygen content of infiltrating recharge, this prolonged residency time in the soil matrix catalyzes the desorption of DRP from legacy sources. In fields with a history of biosolid applications which have created accumulations of legacy P, SBF clearly controls both the release and the transport of DRP.

DRP Mass Transported by Groundwater

Whereas the RRF groundwater flow path carries DRP to the tile drain rapidly, SBF represents slower groundwater transport and discharge over a longer period of time. Results indicate that SBF is the principal flow path responsible for transporting the bulk of DRP mass by groundwater due to the temporal and physical characteristics of the flow path, presenting a new focus for future research.

The mass of DRP advected by groundwater flow to the tile drain was found to be dependent on the rate and volume of groundwater discharged. The regional flow direction towards the tile drain in the north hydraulic zone controls the horizontal direction of advected DRP mass while the temporal parameters of the field scale flow regimes control the volume of DRP mass advected. Given that the saturated thickness of the unconfined aquifer dictates the volume of groundwater discharged, forecasted increases in annual precipitation intensity and frequency for the LEB and MRW have the potential to

increase saturated thickness and groundwater discharge. These hydrologic changes could increase the advective capacity of groundwater to transport DRP from legacy sources.

Of the two flow paths evaluated, SBF was the largest contributor to groundwater discharge and DRP mass advected. This again illustrates the minimal role of RRF in transporting DRP in legacy systems. Numerous studies have focused on the role of preferential flow in mobilizing and transporting TP in and DRP in tile drained fields, yet the emphasis on preferential flow paths which primarily transport TP has excluded the potential of SBF to transport legacy P in these systems.

The spatial distribution of the measured groundwater DRP concentration gradient highlights the advective fronts that are transporting DRP in the unconfined aquifer. Advected DRP has the potential to become re-sequestered by being sorbed back onto soil particles depending on hydrogeochemical parameters of the unconfined aquifer, such as pH, dissolved oxygen, and the chemistry of the mineral surfaces present. Therefore, the potential exists for advective fronts of elevated DRP concentration to be laterally distributed within the capillary fringe and phreatic zone. This could explain both vertically and horizontal spatial variation in STP concentrations observed at soil sampling sites.

It can be assumed that DRP inputs from land areas up gradient from tile drains are being horizontally advected in the unconfined aquifer and potentially laterally distributed long the direction of groundwater flow in advective fronts. In the case of the study area, the north hydraulic zone is drained by the main tile drain which intercepts and redirects the regional groundwater flow path direction. The far north and northwest extents of the field are not proximal to the tile drain and therefore any DRP inputs from those land areas

would be horizontally advected much slower than inputs closer to the drain. The increased distance from the drain allows for the possibility of DRP sequestration and accumulation in advective fronts as groundwater slowly passes through the unconfined aquifer. In fields with closer tile drain spacing and more rapid drainage, the potential for advective fronts is decreased due to limited residency time.

While diffusion and dispersion of DRP was not considered in this study, it is important to note that due to the accelerated velocity of groundwater (1.86 ft/day) these processes were assumed to play a minimal role in overall transport. While in conventional groundwater contamination studies advection, diffusion, and dispersion of a contaminate is assessed, this is due to the delivery mechanism which introduced the contaminate to the groundwater system. In the case of legacy soil P acting as the contaminate source, that source encompasses the spatial area of the field and does not have a specific point of origin as is common in contamination studies. It is assumed that due to the large area of input for DRP in legacy systems combined with rapid drainage and groundwater velocity that advection would be the primary mechanism transporting DRP in tile drained fields.

The results of this study show that groundwater is an important and overlooked advective mechanism that is transporting legacy P to tile drains in legacy systems. In addition to advection of DRP mass to tile drains, the possibility of groundwater contributions to ditches, creeks and streams via interflow and groundwater baseflow remain an overlooked method of DRP transport to waterways. By focusing solely on tile drain effluent in edge of field studies, researchers have neglected the importance of the underlying groundwater flow dynamics at the field scale contributing to the current

exacerbation of DRP loads in the MRW. Future research must account for groundwater mobilization and transport of legacy DRP in the dynamics of legacy systems to better understand this evolving threat to water quality in the MRW and LEB.

Tile Drain Mass Transported vs Mass Transported to Tile Drain

More mass was transported by groundwater than was discharged to the tile drain, raising the possibility of sequestration as the DRP mass moves through the unconfined aquifer. Despite the imbalance in DRP mass transported, the DRP mass transported by the tile drain to the stream was significant considering the long history of conservative land management on site. Measured DRP concentrations in tile effluent were found to occasionally exceed EPA TP criteria, yet some samples were barely at the detection limit. DRP concentrations observed in Blue Creek shared a similar pattern of concentrations. While the DRP mass transported off the field via tile drainage was not exorbitant, the fact that the observed amount of DRP was transported off a field with such a long and steadfast history of conservation practices is surprising.

Tile discharge baseflow was found to transport the majority of DRP mass during the study period, highlighting the advective capacity of SBF to transport DRP to the tile drain. Event flow, especially in tile drained systems, is often considered the main mechanism transporting both TP and DRP in tile drained fields, in overland flow and subsurface drainage. While event flow was found to mobilize and transport DRP in the legacy system studied, the majority of DRP was both advected and discharged by baseflow flow regimes. It is postulated that in legacy systems DRP is primarily

transported by baseflow due to the sequestered source, while in fields with active P fertilizer applications baseflow plays a smaller role compared to overland flow which is mobilizing surface particulate P which has not yet leeched into the soil profile.

As the effects of climate change manifest in the Midwest, increased precipitation will likely mobilize more legacy DRP at the study site and in similar legacy fields throughout the MRW and LEB. Increased recharge will result in increasingly saturated unconfined aquifers which will in turn increase advective capacity of groundwater to transport DRP in the vadose zone. Future mitigation strategies and BMPs need to address the growing danger that legacy sources pose in an altered MRW hydrologic cycle. Potential mitigation strategies which can combat the groundwater advection of DRP and subsequent subsurface runoff at the field scale include: soil inversion and selection of P fixing crops, subsurface permeable P sequestering barriers, and the use of in-line nutrient interceptors that intercept tile drainage and sequester P before it enters waterways.

Chapter Five

Conclusion

The objectives of this study were to characterize the source of legacy DRP and evaluate the transport capacity of two potential groundwater flow regimes to transport DRP mass to subsurface drainage. Results indicate that legacy P is mobilized by infiltrating recharge and is exacerbating DRP mass discharge from the study area. Field scale groundwater flow is the dominant mechanism transporting DRP from its source in the soil profile to subsurface drainage. Of two possible groundwater flow regimes which were theorized to transport DRP, SBF was found to be the dominant flow path. SBF transports the bulk of DRP mass physically by discharge volume and temporally through a regressive discharge rate. The mass budget between tile drain effluent DRP mass and groundwater DRP mass raises questions about the potential fate of DRP as it is advected through the unconfined aquifer. Additional research focused on detailed mapping of both horizontal and vertical flow paths in the unconfined aquifer and soil profile could shed light on the possibility of DRP adsorption as advective fronts proceed, both at this site and other legacy sites in the MRW.

Adopted BMPs centered around soil conservation coupled with increasingly intense and frequent spring and summer precipitation, changing precipitation chemistry, and historical P applications have created a perfect environment for DRP mobilization and transport within the rapidly drained agricultural unconfined aquifers in the MRW and greater LEB. While tile effluent is indicative of direct edge of field contributions, the groundwater parameters controlling transport of DRP to tile drains is an important factor in not only releasing DRP from legacy sources but also in transporting that mass to

subsurface drainage. To fully grasp the impact of legacy P sources on DRP loading in the LEB and MRW, future research must incorporate the regional groundwater influence on the dynamics of DRP at the field scale.

References

Andrade, C., 2013, An Exploratory Study on Heads Up Photo Interpretationof Aerial Photography as a Method for Mapping Drainage Tiles: Papers in Resource Analysis Saint Mary's University of Minnesota, v. 15.

Arhonditsis, G. B., Neumann, A., Shimoda, Y., Kim, D.-K., Dong, F., Onandia, G., Yang, C., Javed, A., Brady, M., Visha, A., Ni, F., and Cheng, V., 2019, Castles built on sand or predictive limnology in action? Part B: Designing the next monitoring-modelling-assessment cycle of adaptive management in Lake Erie: Ecological Informatics, v. 53.

Baker, D. B., Confesor, R., Ewing, D. E., Johnson, L. T., Kramer, J. W., and Merryfield, B. J., 2014, Phosphorus loading to Lake Erie from the Maumee, Sandusky and Cuyahoga rivers: The importance of bioavailability: Journal of Great Lakes Research, v. 40, no. 3, p. 502-517.

Baker, D. B., Johnson, L. T., Confesor, R. B., and Crumrine, J. P., 2017, Vertical Stratification of Soil Phosphorus as a Concern for Dissolved Phosphorus Runoff in the Lake Erie Basin: J Environ Qual, v. 46, no. 6, p. 1287-1295.

Baker, D. B., Johnson, L. T., Confesor, R. B., Crumrine, J. P., Guo, T., and Manning, N. F., 2019, Needed: Early-term adjustments for Lake Erie phosphorus target loads to address western basin cyanobacterial blooms: Journal of Great Lakes Research, v. 45, no. 2, p. 203-211.

Burnett, E., Wilson, R. S., Heeren, A., and Martin, J., 2018, Farmer adoption of cover crops in the western Lake Erie basin: Journal of Soil and Water Conservation, v. 73, no. 2, p. 143-155.

Burnett, E. A., R. S. Wilson, B. Roe, G. Howard, E. Irwin, W. Zhang, and J. Martin, 2015, Farmers, Phosphorus and Water Quality: Part II; A Descriptive Report of Beliefs, Attitudes and Best Management Practices in The Maumee Watershed of The Western Lake Erie Basin: The Ohio State University, v. School of Environment & Natural Resources.

Cober, J. R., Macrae, M. L., and Van Eerd, L. L., 2018, Nutrient Release from Living and Terminated Cover Crops Under Variable Freeze-Thaw Cycles: Agronomy Journal, v. 110, no. 3, p. 1036-1045.

Crosbie, R. S., Binning, P., and Kalma, J. D., 2005, A time series approach to inferring groundwater recharge using the water table fluctuation method: Water Resources Research, v. 41, no. 1.

Culman, S., Fulford, A., Camberato, J., and Steinke, K., 2020, Tri-State Fertilizer Recommendations for Corn, Soybeans, Wheat, and Alfalfa: Bulletin 974.

Daniels, M. B., Sharpley, A., Harmel, R. D., and Anderson, K., 2018, The utilization of edge-of-field monitoring of agricultural runoff in addressing nonpoint source pollution: Journal of Soil and Water Conservation, v. 73, no. 1, p. 1-8.

Domagalski, J. L., 2012, Phosphorus and Groundwater: Establishing Links Between Agricultural Use and Transport to Streams: USGS National Water-Quality Assessment Program.

EPA, 2000, Ambient Water QualityCriteria RecommendationsInformation Supporting the Developmentof State and Tribal Nutrient CriteriaRivers and Streams in Nutrient Ecoregion VI, *in* Water, O. o., ed.: Washington, D.C., U.S. ENVIRONMENTAL PROTECTION AGENCY.

EPA, U. S., 2008, Method 365.3: Phosphorus, All Forms (Colorimetric, Ascorbic Acid, Two Reagent), *in* EPA, U. S., ed.

Fetter, C. W., 2000, Applied Hydrogeology, Pearson.

Gatiboni, L., Brunetto, G., Pavinato, P. S., and George, T. S., 2020, Editorial: Legacy Phosphorus in Agriculture: Role of Past Management and Perspectives for the Future: Frontiers in Earth Science, v. 8.

Guo, T., Johnson, L. T., LaBarge, G. A., Penn, C. J., Stumpf, R. P., Baker, D. B., and Shao, G., 2021, Less Agricultural Phosphorus Applied in 2019 Led to Less Dissolved Phosphorus Transported to Lake Erie: Environ Sci Technol, v. 55, no. 1, p. 283-291.

Hanrahan, B. R., King, K. W., and Williams, M. R., 2021, Controls on subsurface nitrate and dissolved reactive phosphorus losses from agricultural fields during precipitation-driven events: Sci Total Environ, v. 754, p. 142047.

IGS, 2015, Identifying And Mapping Tile Drainage Tutorial Wright County, Iowa, *in* EPA, U., ed., US EPA Special Grant.

IJC, 2018, Fertilizer Application Patterns and Trends and Their Implications for Water Quality in the Western Lake Erie Basin: International Joint Commission (USA & Canada).

Interior Dept., B. o. R., 2001, Water Measurement Manual: A Guide to Effective Water Measurement Practices for Better Water Management, *in* Interior Dept., B. o. R., ed., p. Ch. 7.

Islam, R., and Reeder, R., 2014, No-till and conservation agriculture in the United States: An example from the David Brandt farm, Carroll, Ohio: International Soil and Water Conservation Research, v. 2, no. 1, p. 97-107.

Jarvie, H. P., Johnson, L. T., Sharpley, A. N., Smith, D. R., Baker, D. B., Bruulsema, T. W., and Confesor, R., 2017, Increased Soluble Phosphorus Loads to Lake Erie: Unintended Consequences of Conservation Practices?: J Environ Qual, v. 46, no. 1, p. 123-132.

Kane, D. D., Conroy, J. D., Peter Richards, R., Baker, D. B., and Culver, D. A., 2014, Re-eutrophication of Lake Erie: Correlations between tributary nutrient loads and phytoplankton biomass: Journal of Great Lakes Research, v. 40, no. 3, p. 496-501.

Kast, J. B., Apostel, A. M., Kalcic, M. M., Muenich, R. L., Dagnew, A., Long, C. M., Evenson, G., and Martin, J. F., 2021, Source contribution to phosphorus loads from the Maumee River watershed to Lake Erie: J Environ Manage, v. 279, p. 111803.

King, K. W., Williams, M. R., and Fausey, N. R., 2015, Contributions of systematic tile drainage to watershed-scale phosphorus transport: J Environ Qual, v. 44, no. 2, p. 486-494.

-, 2016, Effect of crop type and season on nutrient leaching to tile drainage under a corn-soybean rotation: Journal of Soil and Water Conservation, v. 71, no. 1, p. 56-68.

King, K. W., Williams, M. R., LaBarge, G. A., Smith, D. R., Reutter, J. M., Duncan, E. W., and Pease, L. A., 2018, Addressing agricultural phosphorus loss in artificially drained landscapes with 4R nutrient management practices: Journal of Soil and Water Conservation, v. 73, no. 1, p. 35-47.

Liu, J., Macrae, M. L., Elliott, J. A., Baulch, H. M., Wilson, H. F., and Kleinman, P. J. A., 2019a, Impacts of Cover Crops and Crop Residues on Phosphorus Losses in Cold Climates: A Review: J Environ Qual, v. 48, no. 4, p. 850-868.

Liu, Y., Wang, R., Guo, T., Engel, B. A., Flanagan, D. C., Lee, J. G., Li, S., Pijanowski, B. C., Collingsworth, P. D., and Wallace, C. W., 2019b, Evaluating efficiencies and cost-effectiveness of best management practices in improving agricultural water quality using integrated SWAT and cost evaluation tool: Journal of Hydrology, v. 577.

Marsily, G., 1985, Quantitative Hydrogeology: Groundwater Hydrology for Engineers.

Meybloom, P., 1961, Estimating Ground-Water Recharge from Stream Hydrographs: Journal of Geophysical Research, v. 66 (4), p. 1203-1214.

Michalak, A. M., Anderson, E. J., Beletsky, D., Boland, S., Bosch, N. S., Bridgeman, T. B., Chaffin, J. D., Cho, K., Confesor, R., Daloglu, I., Depinto, J. V., Evans, M. A., Fahnenstiel, G. L., He, L., Ho, J. C., Jenkins, L., Johengen, T. H., Kuo, K. C., Laporte, E., Liu, X., McWilliams, M. R., Moore, M. R., Posselt, D. J., Richards, R. P., Scavia, D., Steiner, A. L., Verhamme, E., Wright, D. M., and Zagorski, M. A., 2013, Record-setting algal bloom in Lake Erie caused by agricultural and meteorological trends consistent with expected future conditions: Proc Natl Acad Sci U S A, v. 110, no. 16, p. 6448-6452.

Muenich, R. L., Kalcic, M., and Scavia, D., 2016, Evaluating the Impact of Legacy P and Agricultural Conservation Practices on Nutrient Loads from the Maumee River Watershed: Environ Sci Technol, v. 50, no. 15, p. 8146-8154.

Ni, X., Yuan, Y., and Liu, W., 2020, Impact factors and mechanisms of dissolved reactive phosphorus (DRP) losses from agricultural fields: A review and synthesis study in the Lake Erie basin: Sci Total Environ, v. 714, p. 136624.

Osterholz, W., King, K., Williams, M., Hanrahan, B., and Duncan, E., 2020a, Stratified Soil Sampling Improves Predictions of P Concentration in Surface Runoff and Tile Discharge: Soil Systems, v. 4, no. 4.

Osterholz, W. R., Hanrahan, B. R., and King, K. W., 2020b, Legacy phosphorus concentration-discharge relationships in surface runoff and tile drainage from Ohio crop fields: J Environ Qual, v. 49, no. 3, p. 675-687.

Pease, L. A., King, K. W., Williams, M. R., LaBarge, G. A., Duncan, E. W., and Fausey, N. R., 2018, Phosphorus export from artificially drained fields across the Eastern Corn Belt: Journal of Great Lakes Research, v. 44, no. 1, p. 43-53.

Pierzynski, G., 2000, Methods of Phosphorus Analysis for Soils, Sediments, Residuals, and Waters: Southern Cooperative Series Bulletin, v. 396, p. 91-93.

Pizarro, A., 1988, Determination of the Strike and Dip of Planar Geologic Structures: A Computer Solution: Journal of Computers in Mathematics and Science Teaching, v. 7(3), no. Spring, p. 59-61.

Sharpley, A., Jarvie, H. P., Buda, A., May, L., Spears, B., and Kleinman, P., 2013, Phosphorus legacy: overcoming the effects of past management practices to mitigate future water quality impairment: J Environ Qual, v. 42, no. 5, p. 1308-1326.

Sharpley, A. N., Kleinman, P. J., Jordan, P., Bergstrom, L., and Allen, A. L., 2009, Evaluating the success of phosphorus management from field to watershed: J Environ Qual, v. 38, no. 5, p. 1981-1988.

Smith, D. R., Francesconi, W., Livingston, S. J., and Huang, C. H., 2015a, Phosphorus losses from monitored fields with conservation practices in the Lake Erie Basin, USA: Ambio, v. 44 Suppl 2, p. S319-331.

Smith, D. R., King, K. W., Johnson, L., Francesconi, W., Richards, P., Baker, D., and Sharpley, A. N., 2015b, Surface runoff and tile drainage transport of phosphorus in the midwestern United States: J Environ Qual, v. 44, no. 2, p. 495-502.

Smith, D. R., King, K. W., and Williams, M. R., 2015c, What is causing the harmful algal blooms in Lake Erie?: Journal of Soil and Water Conservation, v. 70, no. 2, p. 27A-29A.

Smith, D. R., Stephensen, M., King, K. W., Jarvie, H. P., Haney, R., and Williams, M. R., 2017, A possible trade-off between clean air and clean water: Journal of Soil and Water Conservation, v. 72, no. 4, p. 75A-79A.

Thompson, J., 2010, Identifying subsurface tile drainage systems utilizing remote sensing techniques: University of Toledo.

Vacher, H. L., 1989, The Three-Point Problem in the Context of Elementary Vector Analysis: Journal of Geological Education, v. 37, no. 4, p. 280-287.

Williams, M. R., King, K. W., Baker, D. B., Johnson, L. T., Smith, D. R., and Fausey, N. R., 2016a, Hydrologic and biogeochemical controls on phosphorus export from Western Lake Erie tributaries: Journal of Great Lakes Research, v. 42, no. 6, p. 1403-1411.

Williams, M. R., King, K. W., Ford, W., Buda, A. R., and Kennedy, C. D., 2016b, Effect of tillage on macropore flow and phosphorus transport to tile drains: Water Resources Research, v. 52, no. 4, p. 2868-2882.

Yuan, Y., Ni, X., and Liu, W., 2020, Dissolved Reactive Phosphorus Losses from Agricultural Fields in the Lake Erie Basin: A Synthesis.

Appendix A

Piezometer Characteristics

Table A-1: Piezometer characteristics including aquifer and aquitard elevations constructed from bore logs. Aquifer thickness was calculated by subtracting the elevation of the aquitard from the average elevation of the potentiometric surface.

Well #	Total Depth Down Well (Ft)	Stick-up (Ft)	Well Head Elevation (Ft)	Well Bottom Elevation (Ft)	Surface Elevation (Ft)	Aquitard Elevation (Ft)	Aquifer thickness (Ft)
BC-01	5.48	2.08	655.601	650.12	653.521	648.2	5.321
BC-02	8.29	2.3	656.871	648.58	654.571	648.5	6.071
BC-03	7.55	1.7	652.261	644.71	650.561	645.12	5.441
BC-04	7.4	2.2	649.891	642.49	647.691	638.2	9.491
BC-05	4.71	0	649.281	644.57	649.281	644.6	4.681
BC-06	7.565	2	645.741	638.18	643.741	637.4	6.341
BC-07	8.275	2.194	647.111	638.84	644.917	639.2	5.717
BC-08	7.08	1.21	645.031	637.95	643.821	637.5	6.321
BC-09	5.04	2	645.151	640.11	643.151	640	3.151
BC-10	4.91	0	653.681	648.77	653.681	642.6	11.081
BC-11	6.09	1.6	655.851	649.76	654.251	645.8	8.451
BC-12	5.15	0	653.211	648.06	653.211	644.2	9.011
BC-13	6.25	0	651.401	645.15	651.401	644.2	7.201
BC-14	6.2	2	645.981	639.78	643.981	638.4	5.581
BC-15	5.945	2	652.131	646.19	650.131	648.9	1.231

Appendix B

All Measured DRP Concentrations

Figure B-1: Average DRP concentrations (mg/L) present in groundwater collected from indicated piezometers.

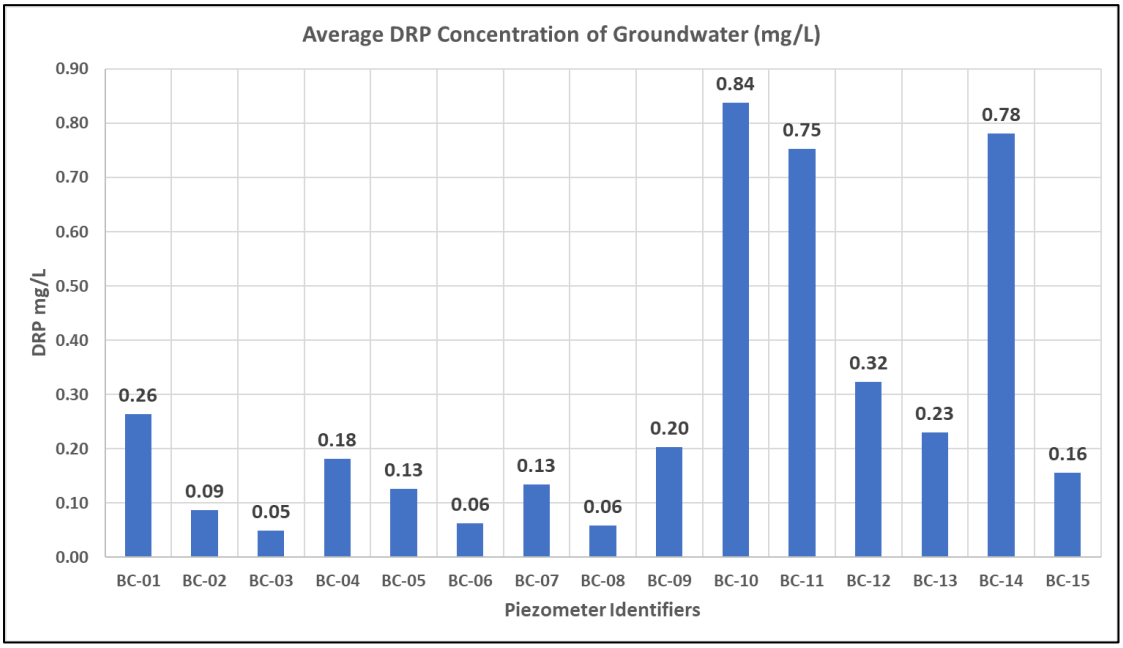

Figure B-2: Tile drain effluent DRP concentrations (mg/L) for the study period. Note the high frequency sampling on 5/19/21-5/20/21 during a storm event.

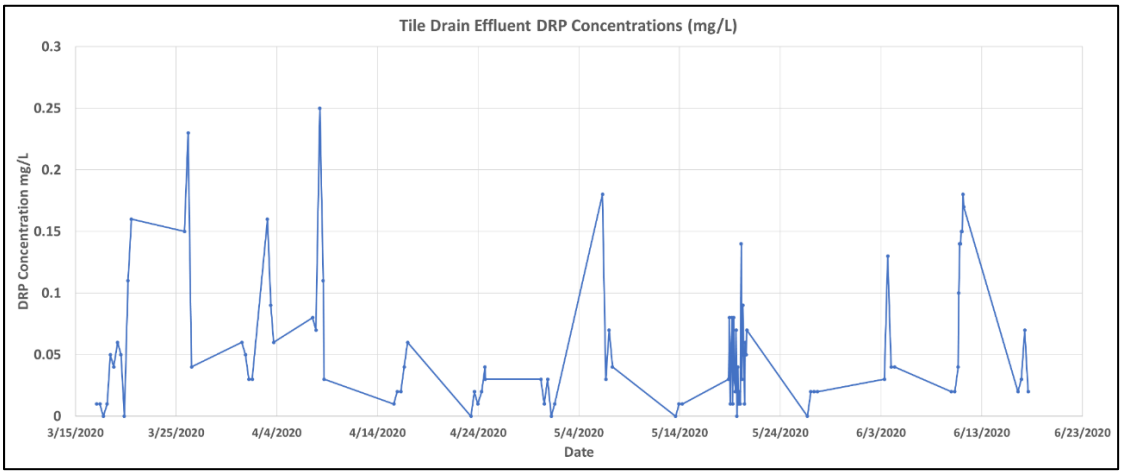

Figure B-3: Measured DRP concentrations for Blue Creek (mg/L)

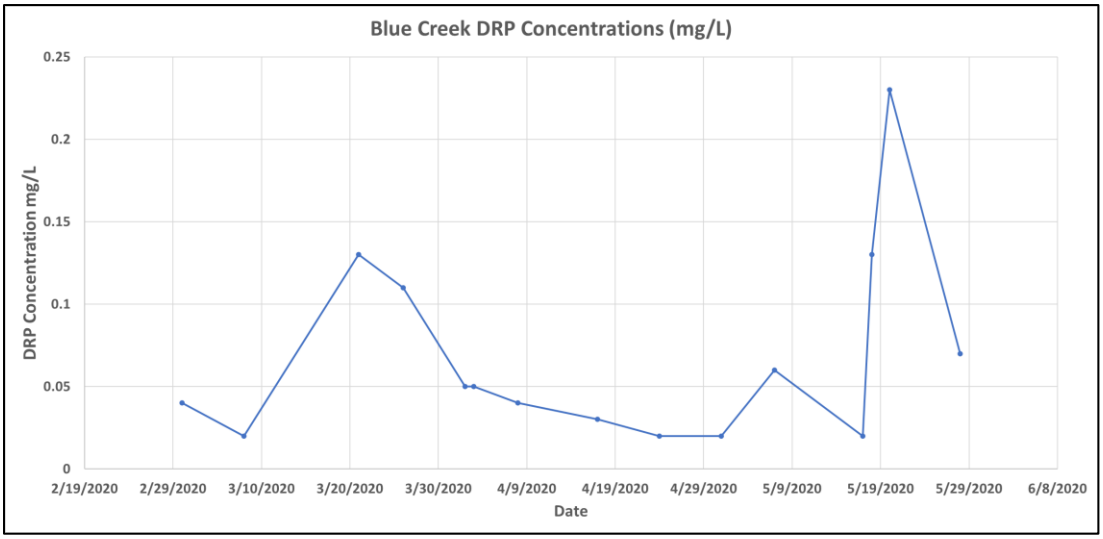

Appendix C

DRP Mass & Discharge Tables for Piezometer Triangles

*Tables of piezometer triangles #1-#16. Tables include: Gradient direction, gradient, saturated aquifer thickness at each of the three piezometers constituting the triangle, average saturated thickness, flux, volumetric discharge, DRP concentration at each piezometer constituting the triangle, average DRP concentration for that day, and the total DRP mass transport rate per day.

Table C-1: Triangle 1

Date	BC-01 (ft)	BC-12 (ft)	BC-11 (ft)	Grad Dir	Grad.h	b_{01} (ft)	b_{12} (ft)	b_{11} (ft)	b_{av} (ft)	q' (ft^2/d)	Q (ft^3/d)	C_{01} (g/ft^3)	C_{12}	C_{11}	C_{av}	M (g/d)
3/6/2020	651.576	651.651	651.78	324.4	0.000632	3.376	7.451	5.98	5.602333	1.33E-07	4.26E+00	0.00154	0.00227	0.02593	0.009913	4.22E-02
3/13/2020	651.203	650.636	651.453	16.5	0.004380	3.003	6.436	5.653	5.030667	8.29E-07	2.65E+01	0.00407	0.00227	0.02973	0.012023	3.19E-01
3/20/2020	652.891	652.131	653.341	14.3	0.006345	4.691	7.931	7.541	6.721	1.60E-06	5.13E+01	0.00819	0.01331	0.03766	0.01972	1.01E+00
4/1/2020	651.702	652.71	652.311	228.9	0.004132	3.502	8.51	6.511	6.174333	9.59E-07	3.07E+01	0.0072	0.01642	0.02678	0.0168	5.15E-01
4/8/2020	652.306	652.691	653.171	316.3	0.002510	4.106	8.491	7.371	6.656	6.28E-07	2.01E+01	0.00906	0.02095	0.03653	0.02218	4.46E-01
4/24/2020	650.816	649.796	651.271	16.4	0.007901	2.616	5.596	5.471	4.561	1.36E-06	4.33E+01	0.00623	0.01218	0.04701	0.021807	9.45E-01
5/1/2020	652.825	649.416	651.051	44.5	0.014678	4.625	5.216	5.251	5.030667	2.78E-06	8.88E+01	0.00737	0.02148	0.01019	0.013012	1.16E+00
5/20/2020	652.281	649.421	653.111	19.0	0.020355	4.081	5.221	7.311	5.537667	4.24E-06	1.36E+02	0.01048	0.00906	0.03087	0.016804	2.28E+00

Table C-2: Triangle 2

Date	BC-10 (ft)	BC-12 (ft)	BC-11 (ft)	Grad Dir	Grad.h	b_{01} (ft)	b_{12} (ft)	b_{11} (ft)	b_{av} (ft)	q' (ft^2/d)	Q (ft^3/d)	C_{01} (g/ft^3)	C_{12}	C_{11}	C_{av}	M (g/d)
3/13/2020	651.121	650.636	651.453	317.3	0.004232	7.521	7.253	5.653	6.809	1.08E-06	2.73E+01	0.01958	0.00227	0.02973	0.017193	4.69E-01
3/20/2020	653.131	652.131	653.341	307.5	0.006999	9.531	9.141	7.541	8.737667	2.30E-06	5.79E+01	0.03694	0.01331	0.03766	0.029303	1.70E+00
4/1/2020	651.28	652.71	652.311	90.5	0.006916	7.68	8.111	6.511	7.434	1.93E-06	4.87E+01	0.0294	0.01642	0.02678	0.0242	1.18E+00
4/8/2020	651.571	652.691	653.171	53.6	0.005977	7.971	8.971	7.371	8.104333	1.82E-06	4.58E+01	0.03794	0.02095	0.03653	0.031807	1.46E+00
4/24/2020	650.111	649.796	651.271	337.7	0.006815	6.511	7.071	5.471	6.351	1.63E-06	4.10E+01	0.03171	0.01218	0.04701	0.0303	1.24E+00
5/1/2020	649.831	649.416	651.051	335.3	0.007601	6.231	6.851	5.251	6.111	1.75E-06	4.40E+01	0.01557	0.02148	0.01019	0.015746	6.92E-01
5/20/2020	650.451	649.421	653.111	333.9	0.017237	6.851	8.911	7.311	7.691	4.98E-06	1.25E+02	0.03483	0.00906	0.03087	0.02492	3.13E+00

Table C-3: Triangle 3

Date	BC-10 (ft)	BC-12 (ft)	BC-09 (ft)	Grad Dir	Grad.h	b_{01} (ft)	b_{12} (ft)	b_{11} (ft)	b_{av} (ft)	q' (ft^2/d)	Q (ft^3/d)	C_{01} (g/ft^3)	C_{12}	C_{11}	C_{av}	M (g/d)
3/13/2020	651.121	650.636	641.249	218.9	0.034475	7.521	6.436	1.249	5.068667	6.57E-06	2.16E+02	0.01958	0.00227	0.00765	0.009833	2.12E+00
3/20/2020	653.131	652.131	642.841	216.3	0.035765	9.531	7.931	2.841	6.767667	9.10E-06	2.99E+02	0.03694	0.01331	0.00963	0.01996	5.97E+00
4/1/2020	651.28	652.71	642.283	229.6	0.032766	7.68	8.51	2.283	6.157667	7.59E-06	2.49E+02	0.0294	0.01642	0.00756	0.017793	4.44E+00
4/8/2020	651.571	652.691	642.501	227.8	0.032723	7.971	8.491	2.501	6.321	7.78E-06	2.56E+02	0.03794	0.02095	0.00708	0.02199	5.62E+00
4/24/2020	650.111	649.796	641.056	219.7	0.031679	6.511	5.596	1.056	4.387667	5.23E-06	1.72E+02	0.03171	0.01218	0.00595	0.016613	2.85E+00
5/1/2020	649.831	649.416	640.671	219.1	0.032004	6.231	5.216	0.671	4.039333	4.86E-06	1.60E+02	0.01557	0.02148	0.00057	0.012539	2.00E+00
5/20/2020	650.451	649.421	643.462	213.6	0.024223	6.851	5.221	3.462	5.178	4.72E-06	1.55E+02	0.03483	0.00906	0.01501	0.021946	3.40E+00

Table C-4: Triangle 4

Date	BC-07 (ft)	BC-12 (ft)	BC-09 (ft)	Grad Dir	Grad.h	b_{01} (ft)	b_{12} (ft)	b_{11} (ft)	b_{av} (ft)	q' (ft^2/d)	Q (ft^3/d)	C_{01} (g/ft^3)	C_{12}	C_{11}	C_{av}	M (g/d)
3/13/2020	641.746	650.636	641.249	202.8	0.050564	2.746	6.436	1.249	3.477	6.61E-06	1.90E+02	0.00318	0.00227	0.00765	0.004367	8.28E-01
3/20/2020	643.496	652.131	642.841	203.4	0.049123	4.496	7.931	2.841	5.089333	9.40E-06	2.70E+02	0.00288	0.01331	0.00963	0.008607	2.32E+00
4/1/2020	642.99	652.71	642.283	203.3	0.055294	3.99	8.51	2.283	4.927667	1.02E-05	2.94E+02	0.00328	0.01642	0.00756	0.009087	2.67E+00
4/8/2020	643.351	652.691	642.501	203.8	0.053145	4.351	8.491	2.501	5.114333	1.02E-05	2.93E+02	0.00176	0.02095	0.00708	0.00993	2.91E+00
4/24/2020	641.536	649.796	641.056	202.9	0.046982	2.536	5.596	1.056	3.062667	5.41E-06	1.55E+02	0.00255	0.01218	0.00595	0.006893	1.07E+00
5/1/2020	641.216	649.416	640.671	203.1	0.046644	2.216	5.216	0.671	2.701	4.74E-06	1.36E+02	0.00085	0.02148	0.00057	0.007632	1.04E+00
5/7/2020	640.901	649.021	640.261	203.5	0.046195	1.901	4.821	0.261	2.327667	4.04E-06	1.16E+02	0.0051	0.02945	0.00078	0.011776	1.37E+00
5/20/2020	643.711	649.421	643.462	202.4	0.032475	4.711	5.221	3.462	4.464667	5.45E-06	1.56E+02	0.00963	0.00906	0.01501	0.011234	1.76E+00

Table C-5: Triangle 5

Date	BC-02 (ft)	BC-05 (ft)	BC-03 (ft)	Grad Dir	Grad.h	b_{01} (ft)	b_{12} (ft)	b_{11} (ft)	b_{av} (ft)	q' (ft^2/d)	Q (ft^3/d)	C_{01} (g/ft^3)	C_{12}	C_{11}	C_{av}	M (g/d)
3/6/2020	650.396	646.6145	647.846	191.3	0.010448	2.196	2.0145	2.726	2.312167	9.08E-07	2.76E+01	0.00085	0.00073	0.00085	0.00081	2.24E-02
3/13/2020	650.209	646.166	647.561	192.5	0.011216	2.009	1.566	2.441	2.005333	8.46E-07	2.57E+01	0.0027	0.00078	0.00063	0.00137	3.52E-02
3/20/2020	651.438	646.816	649.11	201.3	0.013409	3.238	2.216	3.99	3.148	1.59E-06	4.82E+01	0.00529	0.00109	0.00033	0.002237	1.08E-01
4/1/2020	650.651	647.451	647.951	180.6	0.008695	2.451	2.851	2.831	2.711	8.86E-07	2.69E+01	0.00376	0.0084	0.0021	0.004753	1.28E-01
4/8/2020	650.811	647.241	648.251	188.6	0.009790	2.611	2.641	3.131	2.794333	1.03E-06	3.13E+01	0.00538	0.00113	0.00028	0.002263	7.07E-02
4/24/2020	650.001	645.771	647.081	190.3	0.011652	1.801	1.171	1.961	1.644333	7.20E-07	2.19E+01	0.00057	0.00651	0.0017	0.002927	6.41E-02
5/1/2020	649.851	645.321	646.776	191.0	0.012505	1.651	0.721	1.656	1.342667	6.31E-07	1.92E+01	0.00113	0.00198	0.00028	0.00113	2.17E-02
5/7/2020	649.781	644.921	646.471	190.9	0.013410	1.581	0.321	1.351	1.084333	5.47E-07	1.66E+01	0.00085	0.00510	0.00142	0.002457	4.08E-02
5/20/2020	650.432	645.65	647.651	196.9	0.013519	2.232	1.05	2.531	1.937667	9.85E-07	2.99E+01	0.00538	0.00396	0.0017	0.00368	1.10E-01

Table C-6: Triangle 6

Date	BC-06 (ft)	BC-05 (ft)	BC-13 (ft)	Grad Dir	Grad.h	b_{01} (ft)	b_{12} (ft)	b_{11} (ft)	b_{av} (ft)	q' (ft^2/d)	Q (ft^3/d)	C_{01} (g/ft^3)	C_{12}	C_{11}	C_{av}	M (g/d)
3/13/2020	641.669	646.166	648.802	51.6	0.018795	4.269	1.566	3.602	3.145667	2.22E-06	1.07E+02	0.00028	0.00078	0.00407	0.00171	1.83E-01
3/20/2020	643.581	646.816	650.886	40.2	0.024178	6.181	2.216	5.686	4.694333	4.27E-06	2.06E+02	0.00028	0.00109	0.00621	0.002527	5.20E-01
4/1/2020	642.851	647.451	650.881	47.5	0.022718	5.451	2.851	5.681	4.661	3.98E-06	1.92E+02	0.00028	0.0084	0.00971	0.00613	1.18E+00
4/8/2020	643.741	647.241	649.821	47.7	0.017141	6.341	2.641	4.621	4.534333	2.92E-06	1.41E+02	0.00028	0.00113	0.00878	0.003397	4.79E-01
4/24/2020	641.161	645.771	647.986	55.2	0.017021	3.761	1.171	2.786	2.572667	1.65E-06	7.94E+01	0.00113	0.00651	0.0051	0.004247	3.37E-01
5/1/2020	640.961	645.321	647.606	53.6	0.016966	3.561	0.721	2.406	2.229333	1.42E-06	6.86E+01	0.00028	0.00198	0.00372	0.001993	1.37E-01
5/7/2020	640.821	644.921	647.071	53.6	0.015960	3.421	0.321	1.871	1.871	1.12E-06	5.41E+01	0.00170	0.00510	0.00255	0.003117	1.69E-01
5/20/2020	644.321	645.65	647.661	38.1	0.011644	6.921	1.05	2.461	3.477333	1.52E-06	7.34E+01	0.00227	0.00396	0.00708	0.004437	3.26E-01

Table C-7: Triangle 7

Date	BC-06 (ft)	BC-05 (ft)	BC-15 (ft)	Grad Dir	Grad.h	b_{01} (ft)	b_{12} (ft)	b_{11} (ft)	b_{av} (ft)	q' (ft^2/d)	Q (ft^3/d)	C_{01} (g/ft^3)	C_{12}	C_{11}	C_{av}	M (g/d)
3/20/2020	643.581	646.816	647.071	67.7	0.007551	6.181	2.216	1.951	3.449333	9.79E-07	4.36E+01	0.00028	0.00109	0.00623	0.002533	1.11E-01
4/1/2020	642.851	647.451	645.821	31.5	0.012621	5.451	2.851	0.701	3.001	1.42E-06	6.35E+01	0.00028	0.0084	0.007079	0.005253	3.33E-01
4/8/2020	643.741	647.241	646.246	36.4	0.009149	6.341	2.641	1.126	3.369333	1.16E-06	5.16E+01	0.00028	0.00113	0.004248	0.001886	9.74E-02

Table C-8: Triangle 8

Date	BC-01 (ft)	BC-12 (ft)	BC-02 (ft)	Grad Dir	Grad.h	b_{01} (ft)	b_{12} (ft)	b_{11} (ft)	b_{av} (ft)	q' (ft^2/d)	Q (ft^3/d)	C_{01} (g/ft^3)	C_{12}	C_{11}	C_{av}	M (g/d)
3/6/2020	651.576	651.651	650.396	84.6	0.003719	3.376	7.451	2.196	4.341	6.07E-07	1.77E+01	0.00154	0.00227	0.00085	0.001553	2.75E-02
3/13/2020	651.203	650.636	650.209	152.4	0.003373	3.003	6.436	2.009	3.816	4.84E-07	1.41E+01	0.00407	0.00227	0.0027	0.003013	4.25E-02
3/20/2020	652.891	652.131	651.438	148.5	0.004702	4.691	7.931	3.238	5.286667	9.35E-07	2.72E+01	0.00819	0.01331	0.00529	0.00893	2.43E-01
4/1/2020	651.702	652.71	650.651	47.2	0.007663	3.502	8.51	2.451	4.821	1.39E-06	4.05E+01	0.0072	0.01642	0.00376	0.009127	3.69E-01
4/8/2020	652.306	652.691	650.811	70.2	0.005748	4.106	8.491	2.611	5.069333	1.10E-06	3.19E+01	0.00906	0.02095	0.00538	0.011797	3.76E-01
4/24/2020	650.816	649.796	650.001	180.9	0.005340	2.616	5.596	1.801	3.337667	6.70E-07	1.95E+01	0.00623	0.01218	0.00057	0.006327	1.24E-01
5/1/2020	652.825	649.416	649.851	178.5	0.017860	4.625	5.216	1.651	3.830667	2.57E-06	7.49E+01	0.00737	0.02148	0.00113	0.009992	7.49E-01
5/20/2020	652.281	649.421	650.432	185.9	0.015034	4.081	5.221	2.232	3.844667	2.17E-06	6.33E+01	0.01048	0.00906	0.00538	0.008307	5.26E-01

Table C-9: Triangle 9

Date	BC-02' (ft)	BC-12 (ft)	BC-13' (ft)	Grad Dir	Grad.h	b_{01} (ft)	b_{12} (ft)	b_{11} (ft)	b_{av} (ft)	q' (ft^2/d)	Q (ft^3/d)	C_{01} (g/ft^3)	C_{12}	C_{11}	C_{av}	M (g/d)
3/6/2020	650.396	651.651	649.451	4.5	0.016027	2.196	7.451	4.251	4.632667	2.79E-06	8.48E+01	0.00085	0.00227	0.00247	0.001863	1.58E-01
3/13/2020	650.209	650.636	648.802	12.1	0.013679	2.009	6.436	3.602	4.015667	2.07E-06	6.28E+01	0.0027	0.00227	0.00407	0.003013	1.89E-01
3/20/2020	651.438	652.131	650.886	4.8	0.009075	3.238	7.931	5.686	5.618333	1.92E-06	5.82E+01	0.00529	0.01331	0.00621	0.00827	4.82E-01
4/1/2020	650.651	652.71	650.881	351.5	0.013344	2.451	8.51	5.681	5.547333	2.78E-06	8.46E+01	0.00376	0.01642	0.00971	0.009963	8.43E-01
4/8/2020	650.811	652.691	649.821	2.5	0.020843	2.611	8.491	4.621	5.241	4.11E-06	1.25E+02	0.00538	0.02095	0.00878	0.011703	1.46E+00
4/24/2020	650.001	649.796	647.986	19.5	0.014060	1.801	5.596	2.786	3.394333	1.79E-06	5.45E+01	0.00057	0.01218	0.0051	0.00595	3.24E-01
5/1/2020	649.851	649.416	647.606	22.1	0.014321	1.651	5.216	2.406	3.091	1.66E-06	5.06E+01	0.00113	0.02148	0.00372	0.008776	4.44E-01
5/7/2020	649.781	649.021	647.071	24.9	0.015797	1.581	4.821	1.871	2.757667	1.64E-06	4.98E+01	0.00085	0.02945	0.00255	0.01095	5.45E-01
5/20/2020	650.432	649.421	647.661	28.3	0.014716	2.232	5.221	2.461	3.304667	1.83E-06	5.56E+01	0.00538	0.00906	0.00708	0.007174	3.99E-01

Table C-10: Triangle 10

Date	BC-07 (ft)	BC-12 (ft)	BC-13' (ft)	Grad Dir	Grad.h	b_{01} (ft)	b_{12} (ft)	b_{11} (ft)	b_{av} (ft)	q' (ft^2/d)	Q (ft^3/d)	C_{01} (g/ft^3)	C_{12}	C_{11}	C_{av}	M (g/d)
3/13/2020	641.746	650.636	648.802	63.0	0.031019	2.746	6.436	3.602	4.261333	4.97E-06	1.35E+02	0.00318	0.00227	0.00407	0.003173	4.30E-01
3/20/2020	643.496	652.131	650.886	70.1	0.028750	4.496	7.931	5.686	6.037667	6.53E-06	1.78E+02	0.00288	0.01331	0.00621	0.007467	1.33E+00
4/1/2020	642.99	652.71	650.881	65.0	0.033410	3.99	8.51	5.681	6.060333	7.61E-06	2.07E+02	0.00328	0.01642	0.00971	0.009803	2.03E+00
4/8/2020	643.351	652.691	649.821	53.0	0.035942	4.351	8.491	4.621	5.821	7.87E-06	2.14E+02	0.00176	0.02095	0.00878	0.010497	2.25E+00
4/24/2020	641.536	649.796	647.986	61.6	0.029145	2.536	5.596	2.786	3.639333	3.99E-06	1.09E+02	0.00255	0.01218	0.0051	0.00661	7.18E-01
5/1/2020	641.216	649.416	647.606	61.4	0.028974	2.216	5.216	2.406	3.279333	3.57E-06	9.74E+01	0.00085	0.02148	0.00372	0.008682	8.45E-01
5/7/2020	640.901	649.021	647.071	59.4	0.029207	1.901	4.821	1.871	2.864333	3.15E-06	8.57E+01	0.0051	0.02945	0.00255	0.012366	1.06E+00
5/20/2020	643.711	649.421	647.661	52.9	0.021996	4.711	5.221	2.461	4.131	3.42E-06	9.31E+01	0.00963	0.00906	0.00708	0.00859	8.00E-01

Table C-11: Triangle 11

Date	BC-07 (ft)	BC-09 (ft)	BC-08 (ft)	Grad Dir	Grad.h	b_{01} (ft)	b_{12} (ft)	b_{11} (ft)	b_{av} (ft)	q' (ft^2/d)	Q (ft^3/d)	C_{01} (g/ft^3)	C_{12}	C_{11}	C_{av}	M (g/d)
3/13/2020	641.746	641.249	641.621	99.1	0.003179	2.746	1.249	4.121	2.705333	3.23E-07	4.33E+00	0.00318	0.00765	0.00109	0.003973	1.72E-02
3/20/2020	643.496	642.841	643.841	136.3	0.004764	4.496	2.841	6.341	4.559333	8.17E-07	1.09E+01	0.00288	0.00963	0.00063	0.00438	4.78E-02
4/1/2020	642.99	642.283	642.721	92.7	0.004623	3.99	2.283	5.221	3.831333	6.66E-07	8.91E+00	0.00328	0.00756	0.00081	0.003883	3.46E-02
4/8/2020	643.351	642.501	644.3	154.5	0.007987	4.351	2.501	6.8	4.550667	1.37E-06	1.83E+01	0.00176	0.00708	0.00085	0.00323	5.90E-02
4/24/2020	641.536	641.056	641.521	110.4	0.003047	2.536	1.056	4.021	2.537667	2.91E-07	3.89E+00	0.00255	0.00595	0.00085	0.003117	1.21E-02
5/1/2020	641.216	640.671	641.011	92.9	0.003560	2.216	0.671	3.511	2.132667	2.85E-07	3.82E+00	0.00085	0.00057	0.00028	0.000567	2.16E-03
5/7/2020	640.901	640.261	640.636	91.1	0.004217	1.901	0.261	3.136	1.766	2.80E-07	3.74E+00	0.0051	0.00078	0.00113	0.002337	8.75E-03
5/20/2020	643.711	643.462	644.431	176.6	0.004535	4.711	3.462	6.931	5.034667	8.58E-07	1.15E+01	0.00963	0.01501	0.00166	0.008767	1.01E-01

Table C-12: Triangle 12

Date	BC-02 (ft)	BC-05 (ft)	BC-13 (ft)	Grad Dir	Grad.h	b_{01} (ft)	b_{12} (ft)	b_{11} (ft)	b_{av} (ft)	q' (ft^2/d)	Q (ft^3/d)	C_{01} (g/ft^3)	C_{12}	C_{11}	C_{av}	M (g/d)
3/6/2020	650.396	646.6145	649.451	50.0	0.019615	2.196	2.0145	4.251	2.8205	2.08E-06	6.32E+01	0.00085	0.00073	0.00247	0.00135	8.53E-02
3/13/2020	650.209	646.166	648.802	53.1	0.019364	2.009	1.566	3.602	2.392333	1.74E-06	5.29E+01	0.0027	0.00078	0.00407	0.002517	1.33E-01
3/20/2020	651.438	646.816	650.886	46.5	0.026512	3.238	2.216	5.686	3.713333	3.70E-06	1.12E+02	0.00529	0.00109	0.00621	0.004197	4.72E-01
4/1/2020	650.651	647.451	650.881	42.5	0.021028	2.451	2.851	5.681	3.661	2.89E-06	8.79E+01	0.00376	0.0084	0.00971	0.00729	6.41E-01
4/8/2020	650.811	647.241	649.821	50.8	0.018116	2.611	2.641	4.621	3.291	2.24E-06	6.81E+01	0.00538	0.00113	0.00878	0.005097	3.47E-01
4/24/2020	650.001	645.771	647.986	58.1	0.018168	1.801	1.171	2.786	1.919333	1.31E-06	3.98E+01	0.00057	0.00651	0.0051	0.00406	1.62E-01
5/1/2020	649.851	645.321	647.606	58.9	0.019136	1.651	0.721	2.406	1.592667	1.15E-06	3.48E+01	0.00113	0.00198	0.00372	0.002277	7.93E-02
5/7/2020	649.781	644.921	647.071	61.8	0.019450	1.581	0.321	1.871	1.257667	9.20E-07	2.79E+01	0.00085	0.00510	0.00255	0.002833	7.92E-02
5/20/2020	650.432	645.65	647.661	62.9	0.018776	2.232	1.05	2.461	1.914333	1.35E-06	4.11E+01	0.00538	0.00396	0.00708	0.005473	2.25E-01

Table C-13: Triangle 13

Date	BC-13	BC-06	BC-08'	Grad Dir	Grad.h	b_{01} (ft)	b_{12} (ft)	b_{11} (ft)	b_{av} (ft)	q' (ft^2/d)	Q (ft^3/d)	C_{01} (g/ft^3)	C_{12}	C_{11}	C_{av}	M (g/d)
3/13/2020	648.802	641.669	641.621	81.0	0.015694	3.602	4.269	4.121	3.997333	2.36E-06	9.32E+01	0.00407	0.00028	0.00109	0.001813	1.69E-01
3/20/2020	650.886	643.581	643.841	76.2	0.016450	5.686	6.181	6.341	6.069333	3.75E-06	1.48E+02	0.00621	0.00028	0.00063	0.002373	3.52E-01
4/1/2020	650.881	642.851	642.721	82.2	0.017593	5.681	5.451	5.221	5.451	3.61E-06	1.42E+02	0.00971	0.00028	0.00081	0.0036	5.13E-01
4/8/2020	649.821	643.741	644.3	70.0	0.014255	4.621	6.341	6.8	5.920667	3.17E-06	1.25E+02	0.00878	0.00028	0.00085	0.003303	4.14E-01
4/24/2020	647.986	641.161	641.521	74.2	0.015543	2.786	3.761	4.021	3.522667	2.06E-06	8.13E+01	0.0051	0.00113	0.00085	0.00236	1.92E-01
5/1/2020	647.606	640.961	641.011	79.4	0.014724	2.406	3.561	3.511	3.159333	1.75E-06	6.91E+01	0.00372	0.00028	0.00028	0.001427	9.86E-02
5/7/2020	647.071	640.821	640.636	83.8	0.013620	1.871	3.421	3.136	2.809333	1.44E-06	5.68E+01	0.00255	0.00170	0.00113	0.001793	1.02E-01
5/20/2020	647.661	644.321	644.431	76.5	0.007509	2.461	6.921	6.931	5.437667	1.54E-06	6.07E+01	0.00708	0.00227	0.00166	0.00367	2.23E-01

Table C-14: Triangle 14

Date	BC-14 (ft)	BC-05 (ft)	BC-03 (ft)	Grad Dir	Grad.h	b_{01} (ft)	b_{12} (ft)	b_{11} (ft)	b_{av} (ft)	q' (ft^2/d)	Q (ft^3/d)	C_{01} (g/ft^3)	C_{12}	C_{11}	C_{av}	M (g/d)
3/13/2020	640.261	646.166	647.561	177.8	0.034001	1.861	1.566	-1.739	0.562667	7.19E-07	2.10E+01	0.01721	0.00078	0.00063	0.006207	1.30E-01
3/20/2020	642.211	646.816	649.11	184.0	0.029813	3.811	2.216	-0.19	1.945667	2.18E-06	6.35E+01	0.0932	0.00109	0.00033	0.03154	2.00E+00
4/1/2020	641.231	647.451	647.951	173.3	0.033407	2.831	2.851	-1.349	1.444333	1.81E-06	5.29E+01	0.05597	0.0084	0.0021	0.022157	1.17E+00
4/8/2020	641.311	647.241	648.251	176.0	0.033150	2.911	2.641	-1.049	1.501	1.87E-06	5.45E+01	0.03285	0.00113	0.00028	0.01142	6.22E-01
5/20/2020	645.891	645.65	647.651	232.2	0.006775	7.491	1.05	-1.649	2.297333	5.85E-07	1.70E+01	0.05975	0.00396	0.0017	0.021803	3.72E-01

Table C-15: Triangle 15

Date	BC-14 (ft)	BC-05 (ft)	BC-15 (ft)	Grad Dir	Grad.h	b_{01} (ft)	b_{12} (ft)	b_{11} (ft)	b_{av} (ft)	q' (ft^2/d)	Q (ft^3/d)	C_{01} (g/ft^3)	C_{12}	C_{11}	C_{av}	M (g/d)
3/20/2020	642.211	646.816	647.071	237.6	0.019343	3.811	2.216	1.951	2.659333	1.93E-06	1.67E-01	0.0932	0.00109	0.00623	0.033507	5.60E-03
4/1/2020	641.231	647.451	645.821	256.3	0.022368	2.831	2.851	0.701	2.127667	1.79E-06	1.55E-01	0.05597	0.0084	0.007079	0.023816	3.68E-03
4/8/2020	641.311	647.241	646.246	250.2	0.022127	2.911	2.641	1.126	2.226	1.85E-06	1.60E-01	0.03285	0.00113	0.004248	0.012743	2.04E-03

Table C-16: Triangle 16

Date	BC-06 (ft)	BC-04 (ft)	BC-15 (ft)	Grad Dir	Grad.h	b_{01} (ft)	b_{12} (ft)	b_{11} (ft)	b_{av} (ft)	q' (ft^2/d)	Q (ft^3/d)	C_{01} (g/ft^3)	C_{12}	C_{11}	C_{av}	M (g/d)
3/20/2020	643.581	645.861	647.071	346.5	0.023436	6.181	7.661	1.951	5.264333	4.64E-06	1.91E+02	0.00028	0.0008495	0.00623	0.002453	4.68E-01
4/1/2020	642.851	645.311	645.821	351.3	0.018654	5.451	7.111	0.701	4.421	3.10E-06	1.28E+02	0.00028	0.0005663	0.007079	0.002642	3.37E-01
4/8/2020	643.741	645.396	646.246	346.7	0.016773	6.341	7.196	1.126	4.887667	3.08E-06	1.27E+02	0.00028	0.0008495	0.004248	0.001792	2.27E-01

Appendix D

Tile Drain Effluent DRP Mass Flow Rate & Total Mass

Table D-1: Tile effluent DRP mass transported during the study period by mass flow rate and total grams of DRP.

DRP Mass Flow Rate	**(g/hr)**	**DRP Mass Totals (g)**	**(g)**
Average RRF Mass Flow Rate	0.025	RRF Total Mass	34.08
Average Baseflow Mass Flow Rate	0.061	Baseflow Total Mass	323.58
Average Total Mass Flow Rate	0.019	Total Mass	357.65